Multi-threshold Image Segmentation using a Multi-strategy Shuffled Frog Leaping Algorithm

Article *in* Expert Systems with Applications · January 2022

DOI: 10.1016/j.eswa.2022.116511

Multi-threshold Image Segmentation using a Multi-strategy Shuffled Frog Leaping Algorithm

Yi Chen[1], Mingjing Wang[2], Ali Asghar Heidari[3], Beibei Shi[4], Zhongyi Hu[2], Qian Zhang[5*], Huiling Chen[2*], Majdi Mafarja[6], Hamza Turabieh[7]

[1] School of Computer Science and Technology, East China Normal University, Shanghai 200062, China (52164500006@stu.ecnu.edu.cn)

[2] College of Computer Science and Artificial Intelligence, Wenzhou University, Wenzhou, Zhejiang 325035, China

(wangmingjing.style@gmail.com, huzhongyi@wzu.edu.cn, chenhuiling.jlu@gmail.com)

[3] School of Surveying and Geospatial Engineering, College of Engineering, University of Tehran, Tehran, Iran

(as_heidari@ut.ac.ir, aliasghar68@gmaill.com)

[4]Affiliated People's Hospital of Jiangsu University, 8 Dianli Road, Zhenjiang, Jiangsu 212000, China (shibeibei1993zjfph@163.com)

[5] Wenzhou University of Technology, Wenzhou 325035, China

(qz_zhangqian@163.com)

[6] Department of Computer Science, Birzeit University, P.O. Box 14, West Bank, Palestine

(mmafarja@birzeit.edu)

[7] Department of Information Technology, College of Computers and Information Technology, P.O. Box 11099, Taif 21944, Taif University, Taif, Saudi Arabia

(h.turabieh@tu.edu.sa)

***Corresponding Author**: Qian Zhang (qz_zhangqian@163.com), Huiling Chen(chenhuiling.jlu@gmail.com)*

Abstract: Medical image segmentation, a complex and fundamental step in medical image processing, can help doctors make more precise decisions on patient diagnosis. Although multi-threshold image segmentation is the most exceptionally fundamental image segmentation technology, it requires complex computing and tends to yield unsatisfactory segmentation results, leading to its limited applications. To solve this problem, in this study, an ensemble multi strategy-driven shuffled frog leaping algorithm with horizontal and vertical crossover search (HVSFLA) is designed for multi-threshold image segmentation. Specifically, a horizontal crossover search enables different frogs to exchange information and guarantee the compelling exploration of each frog. Meanwhile, a vertical crossover search can make frogs in stagnation continue to search actively. Therefore, a better balance between diversification and intensification can be ensured. To evaluate its performance, HVSFLA was compared with a range of state-of-the-art algorithms using CEC 2017 benchmark functions. Furthermore, the performance of HVSFLA was also proved on several Berkeley segmentation datasets 500 (BSDS500). Finally, the proposed algorithm was applied to breast invasive ductal carcinoma cases based on multi-threshold segmentation technique using a non-local means 2D histogram integrated with Kapur's entropy. The experimental results demonstrate that the proposed HVSFLA outperforms a broad array of similar competitors, and thus it has a great potential to be used for medical image segmentation.

Keywords: Medical image segmentation; Multi-threshold image segmentation; Shuffled frog leaping algorithm; Horizontal and vertical crossover search; Kapur's entropy;

1 Introduction

The processing of medical images plays a significant role in practical patient diagnosis and treatment. The most critical stage in this process is the segmentation of medical images, which provides valuable diagnostic assistance to doctors. Image segmentation is performed to divides the image into various disconnected areas based on its characteristics, such as spatial texture or geometric form, in order that continuity or similarities are shown in the same area, but unmistakable contrasts are between different areas. Image segmentation is not only the primary concern in medical image processing but also one of the classic cases in the area of computer vision. In most cases, it is difficult for the techniques to separate the image in compliance with human comprehension.

With the steady growth of computer computing resources, image segmentation has drawn more and more interest from researchers in recent years, (L. Liu, et al., 2021). The image segmentation technology is widely used in numerous sectors, including aerospace technology, product defects detection, biomedicine, smart transport, arms management, and safety monitoring. Threshold-based segmentation, in particular, has gained growing interest among many technologies for image segmentation. Therefore, various methods for multi-threshold segmentation of medical images, especially the approaches that use metaheuristics, have gained further interest. Currently, these metaheuristics has found its application in many fields including feature selection (Y. Zhang, Liu, Wang, Chen, & Li, 2020), wind speed prediction (M. Chen, Zeng, Lu, & Weng, 2019), engineering design problems (H. Zhang, et al., 2020), medical data classification (X. Zhao, et al., 2019), bankruptcy prediction (Yu, et al., 2021), parameter optimization (M. Wang & Chen, 2020), PID optimization control (Zeng, Xie, Chen, & Weng, 2019), gate resource allocation (W, JJ, YJ, & HM, 2020), fault diagnosis of rolling bearings (H. Zhao, Liu, Xu, Deng, & measurement, 2019), detection of foreign fiber in cotton (X. Zhao, et al., 2015), traveling salesman problem (Lai & Zhou, 2020), performance optimization (Ying, Ying, & Ban, 2018), neural network training (Zhile Yang, Li, Guo, Ma, & Zheng, 2018), design of power electronic circuit (X.-F. Liu, Zhan, & Zhang, 2021), energy vehicle dispatch (D. Liang, Zhan, Zhang, & Zhang, 2019), large-scale supply chain network design (Xin Zhang, et al., 2019) and prediction problems in educational field (Jixia Tu, Lin, Chen, Li, & Li, 2019).

A multi-level threshold image segmentation method using the moth-swarm algorithm was developed by Zhou et al. (Y. Zhou, Yang, Ling, & Zhang, 2018). To find the near-optimal MCET thresholds, particle swarm optimization was designed by Yin (P. Y. Yin, 2007). A non-revisiting quantum-behaved particle swarm optimization algorithm for image segmentation was proposed by Yang et al. (Z. Yang & Wu, 2019). Tsai et al. (Tsai, Liu, & Chen, 2012) presented a histogram-based multi-threshold color threshold research algorithm. Wang et al. (Y. Wang, Zhang, & Zhang, 2019) proposed a multi-level cooperative heuristic pigeon threshold optimizer based on the threshold of complex distance. Tang et al. (Tang, Yuan, Sun, Yang, & Gao, 2011) developed an enhanced multi-level minimum cross-entropy threshold (MCET) genetic algorithm to collect tighter thresholds. Feng et al. (Y. Feng, Zhao, Li, Zhang, & Li, 2017) proposed a new 3D Otsu and multi-level picture representation algorithm for medical image segmentation, with desirable characteristics that include stable segmentation performance and excellent noise robustness. To find an optimal threshold of multifaceted image segmentation, Fan et al. (C. Fan, Ouyang, Zhang, & Xiao, 2014) suggested a principle of molecular dynamics optimizer technology (MKTOA). Tang et al. (Tang, Xiao, Wu, Yang, & Luo, 2017) designed multi-level bacterial foraging optimization to improve global search capacity and speed up the convergence of the bacterial foraging algorithm, using the particle swarm algorithm (PSO) in every chemical reaction phase after that.

Qin et al. (J. Qin, Wang, & Qin, 2019) proposed the multi-level threshold method based on subspace elimination optimization. Peng et al. (Peng, Wang, Pérez-Jiménez, & Shi, 2013) suggested a new approach to multi-level thresholds using the tissue P method by. Pare et al. (Pare, Kumar, Bajaj, & Singh, 2016) presented a novel search algorithm for multi-level thresholds color segmentation cases using an improved cuckoo algorithm with various parametric processing techniques. Manikandan et al. (Manikandan, Ramar, Iruthayarajan, & Srinivasagan, 2014) used a real coded genetic algorithm with a synthetic binary crossover applied to segment medical brain pictures with multi-level thresholds. Zhao et al. (D. Zhao, Liu, Yu, Heidari, Wang, Liang, et al., 2021) presented chaotic, random spare ant colony optimization for multi-threshold image segmentation. Kotte et al. (Kotte, Pullakura, & Injeti, 2018) also suggested a multi-level threshold wind-driven adaptive algorithm for brain images segmentation. While a variety of algorithms have been introduced to deal with multi-threshold image segmentation, there is still no satisfactory consistency between the solution and the ability to jump out of local optima. Moreover, no algorithm is all-powerful and can fix any problem as says in a no free lunch principle (Wolpert & Macready, 1997). It should be noted that it is appropriate to use a multi-dimensional threshold segmentation approach or pick several thresholds at the same time to achieve efficient segmentation of the target image if the target image is to be segmented more precisely and finely. However, the time complexity of the threshold segmentation algorithm grows exponentially as the image information dimension or collection threshold increases. Increased time complexity means higher criteria for convergence, accuracy and ability to jump out of local optima. Therefore, in this study, we design a new and efficient image segmentation methodology based on the shuffled frog leaping algorithm (Muzaffar M. Eusuff, 2003) (SFLA). The proposed methodology was finally applied to microscopy segmentation for breast cancer. The SFLA (Muzaffar M. Eusuff, 2003), first proposed by Muzaffar et al. in 2003, has been used in a wide variety of realistic scenarios and achieved relatively unexpected success (Karpagam, Geetha, & Rajan, 2020; Y. Liu, et al., 2021). To the best of our knowledge, few studies have used this methodology to solve this image segmentation problem.

In this study, to further boost the potential of the original SFLA for multi-threshold medical image segmentation of breast invasive ductal carcinoma, a typical common breast cancer, two horizontal and vertical crossover search mechanisms abstracted from the crisscross optimizer (CSO) (Meng, Chen, Yin, & Chen, 2014) are integrated into the original SFLA, called an ensemble multi-strategy-driven SFLA (HVSFLA). In this method, a horizontal crossover search is executed between two different frogs in each frog memeplex. It enables different frogs to exchange information, which can guarantee the effective exploration of each frog and speed up convergence rate. Meanwhile, vertical crossover search can make frogs in stagnation to continue to search actively. Eventually, a better balance between diversification and intensification can be ensured. To evaluate the performance of the HVSFLA, the HVSFLA was compared with a multitude of state-of-the-art algorithms on CEC 2017 benchmark functions. In addition, on several Berkeley segmentation datasets 500 (BSDS500), the performance of the HVSFLA was proven. Finally, the proposed algorithm was applied to microscopy segmentation for breast invasive ductal carcinoma cases, using a non-local 2D histogram combined with the Kapur's entropy method of multi-threshold image segmentation. Furthermore, the low and high threshold levels were both used to thoroughly investigate the performance of the presented algorithm. In addition, to determine the effects of image segmentation, the Peak Signal to Noise Ratio (PSNR) (Huynh-Thu & Ghanbari, 2008), Structural Similarity Index (SSIM) (Wang Zhou, Bovik, Sheikh, & Simoncelli, 2004), and Feature Similarity Index (FSIM) (31) were used, and the mean value, variance and the Wilcoxon signed-rank test (L. Zhang, Zhang, Mou, & Zhang, 2011) were applied to assess the results of the assessment.

The main contributions of this paper are given as follows:

(1) The multi-strategy SFLA (HVSFLA) ensemble is presented for the implementation of multi-threshold image segmentation. This research is the first attempt to develop an improved SFLA approach based on horizontal and vertical crossover search mechanisms abstracted from the cruise optimizer.
(2) The effects of the original SFLA are strengthened in HVSFLA by utilizing unique horizontal and vertical crossover search behaviors, achieving a better balance between intensification and diversification.
(3) The proposed HVSFLA was compared with a range of state-of-the-art algorithms on CEC 2017 benchmark functions, Berkeley 500 (BSDS500), and the case of breast invasive ductal carcinoma. The results demonstrate that the proposed HVSFLA has technical and statistical advantages in multi-threshold image segmentation.

The rest of the paper is structured as follows: the detailed background is given in Section 2. Section 3 describes the proposed algorithm. The experiment results on CEC 2017 benchmark functions and Berkeley datasets 500 (BSDS500) at low and high threshold levels are presented in Section 4. The application of the proposed method to breast invasive ductal carcinoma image segmentation is described in Section 5. Section 6 gives a further discussion on the results shown in Section 4. Finally, the conclusion and future work is summarized in Section 7.

2 Background

2.1 Multilevel thresholding image segmentation

In many image processing problems, segmentation of images is a crucial step that divides an image into many disjoint regions based on its characteristics, displaying continuity or similarities within the same area, but unmistakable contrasts between different areas. Multilevel threshold image segmentation (MTIS) searches for multiple image segmented thresholds for multiple regions. Owing to its characteristics of quick implementation, limited measuring volume, and a relatively high level of efficiency, MTIS has evolved into the most widely used processing technology in image segmentation. The histogram-based segmentation approach is prevalent among different MTIS approaches. It can be divided into a single-dimensional histogram system or a two-dimensional histogram solution, with no spatial image position information used for the single-dimensional histogram method. If the target region covers a small area of the image, the false segmentation effect is so severe that the segmentation product is susceptible to nuisance. A two-dimensional histographic fragmentation approach suggested by Abutaleb (Abutaleb, 1989) combines local average pixels with the original Gray-Level histogram. However, since MTIS uses the two-dimensional histogram, the statistical complexity would be enormous if the systematic approach is explicitly used to find the optimum threshold (69, 70).

Many researchers used swarm intelligence algorithms to help find the optimum threshold and achieved considerable efficiency to prevent this phenomenon. However, Abutaleb's method of producing a two-dimensional histogram does not take certain image specifics into account, such as certain points and edges. Thus, a procedure integrating a 2D histogram with the entropy of Kapur to MTIS is employed in this article. In Figure 1, the comprehensive image segmentation process example is based on this approach by selecting photo 35070 from the Berkeley segmentation dataset 500 (BSDS500). Kapur's method is also an unsupervised automatic thresholding technique, which selects the optimum thresholds using the entropy of segmented classes (Kapur, Sahoo, Wong, & processing, 1985). $[th_1, th_2, th_3, \dots, th_n]$ means the thresholds combination which divides the image into various class. The detailed function of Kapur's method can be expressed as:

$$\mathrm{H}(th_1, th_2, th_3, \dots, th_n) = H_0 + H_1 + H_2 + \cdots + H_n$$
$$H_0 = -\sum_{j=0}^{th_1-1} \frac{p_j}{w_0} ln \frac{p_j}{w_0},\ w_0 = \sum_{j=0}^{th_1-1} p_j$$
$$H_1 = -\sum_{j=th_1}^{th_2-1} \frac{p_j}{w_1} ln \frac{p_j}{w_1},\ w_1 = \sum_{j=th_1}^{th_2-1} p_j \tag{1}$$
$$H_n = -\sum_{j=th_n}^{L-1} \frac{p_j}{w_n} ln \frac{p_j}{w_n},\ w_n = \sum_{j=th_n}^{L-1} p_j$$

where $H_0, H_1, \dots, H_n$ means the entropies of distinct classes, and $w_0, w_1, \dots, w_n$ are the probability of each class. More information can be found in (Kapur, et al., 1985).

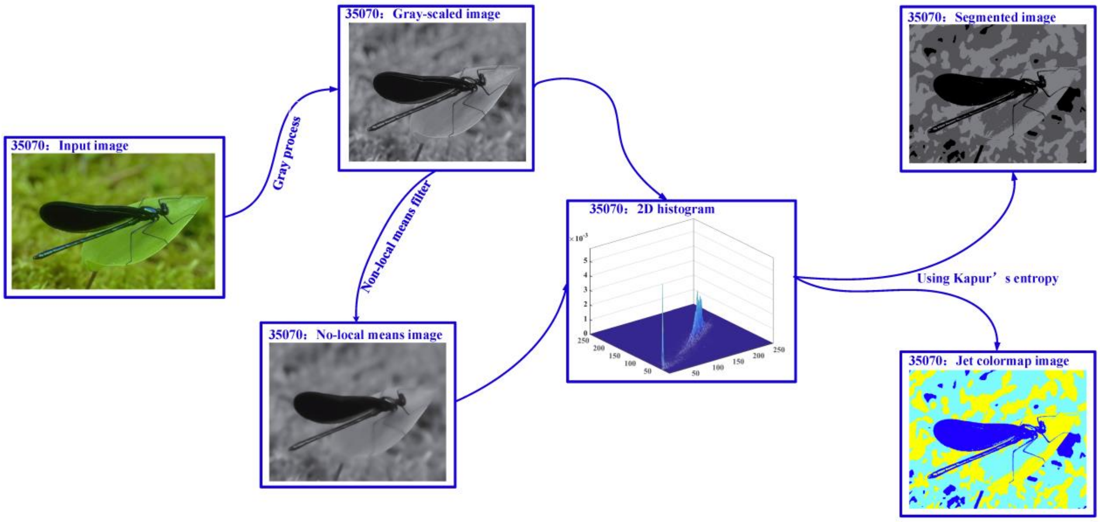

Figure 1. MTIS flowchart with the entropy of Kapur

2.2 Non-local means 2D histogram

Buade et al. (Buades, Coll, & Morel, 2005) developed a non-local medium filtering approach that efficiently eliminates noise by searching for related parts of the pixel or image blocks in the search box and then measuring similar regions' average values. In image H, the non-local average of image H can be determined by Eq. (2) - Eq. (5) in the case of $H(s)$ and $H(t)$ gray scale values that correspond to the pixels s and t.

$$O(s) = \frac{\sum_{s\in H} H(t)\omega(s,t)}{\sum_{s\in H} \omega(s,t)} \tag{2}$$

$$\omega(s,t) = exp^{-\frac{|\mu(s)-\mu(t)|^2}{\sigma^2}} \tag{3}$$

$$\mu(s) = \frac{1}{m\times m} \sum_{i\in L(s)} H(i) \tag{4}$$

$$\mu(t) = \frac{1}{m\times m} \sum_{i\in L(t)} H(i) \tag{5}$$

where

$O(s)$ is the non-local average filter value of pixel s,

$\omega(s,t)$ is the weight of the pixel s and the pixel t,

σ is the standard deviation,

$\mu(s)$ and $\mu(t)$ are the local mean,

$L(s)$ is the $m\times m$ image block centered on s,

$L(t)$ is the $m\times m$ image block centered on t,

The non-local mean is generated by representations from two complex histograms that are non-local, mean, and graying. When an initial grayscale image $H(x,y)$ is of $[0,L-1]$ the magnitude and $M\times N$ size, it is also $[0,L-1]$ magnitude, and of $M\times N$ image size, to be contained in the resultant non-local mean image $g(x,y)$. Furthermore, a plane corresponding to points s (i,j) will form $H(x, y)$ and $g(x, y)$, where *i* denotes pixels in $H(x, y)$ as grayscale and j denotes the pixels in $g(x, y)$, as grayscale value, it is also possible to acquire the number of $h(i, j)$ pixels appearing in the grayscale value vector (*s*, *t*). The respective 2D histogram can then be constructed after normalizing the $h(i, j)$ with equation 6, where $i, j = 0, 1, \cdots, L - 1$ and $\sum_i \sum_j p_{ij} = 1$, $h(i, j)$ denotes the number of times the point (i, j) appears on the grayscale value vector (*s*, *t*) and $M \times N$ is the image size. The significance of equation 6 is to normalize the number of pixel points with the same combination of gray values. In the constructed two-dimensional histogram, the x-axis represents the gray value i of a pixel in the grayscale image, the y-axis represents the gray value j of the same pixel in the non-local mean image, and the z-axis represents the value after normalizing the number of pixel points with the combination of gray values as (i, j) using Eq. (6). The 3D views of 2D histograms generated by non-local mean filtering and color pictures 37073 and 38092 selected from BSDS500 are shown in Figure 2.

$$P_{ij} = \frac{h(i, j)}{M \times N} \tag{6}$$

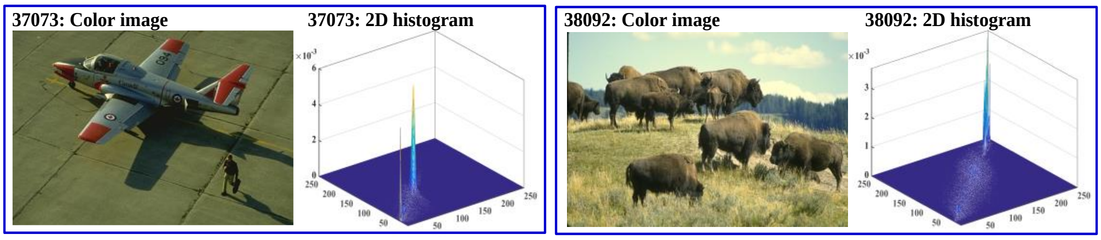

Figure 2. Color images and 3D views of 2D histograms for 12003 and 38082 in BSDS500

2.3 Kapur's entropy for 2D histograms

The associated flat histogram is shown in Figure 3, after the definition of the two-dimensional, non-local medium histogram in section 2.2, where $\{p_1, p_2 \ldots, L - 1\}$ is the value of the grayscale of the gray image, and $\{q_1, q_2 \ldots, L - 1\}$ means the non-local medium image grayscale value. As the main diagonal of a 2D histogram, most image information is contained and is therefore measured easily; Kapur's entropy can only be calculated on the main diagonal for n subregions; the entropy can thus be described as equation 7 for the Kapur image.

$$\varphi(p, q) = -\sum_{i=0}^{p_1} \sum_{j=0}^{q_1} \frac{u_{ij}}{u_1} \ln \frac{v_{ij}}{v_1} - \sum_{i=t_1+1}^{p_2} \sum_{j=t_1+1}^{q_2} \frac{u_{ij}}{u_2} \ln \frac{v_{ij}}{v_2} - \\ \ldots \sum_{i=s_{L-2}+1}^{p_{L-1}} \sum_{j=t_{L-2}+1}^{q_{L-1}} \frac{u_{ij}}{u_{L-1}} \ln \frac{v_{ij}}{v_{L-1}} \tag{7}$$

where $u_1 = \sum_{i=0}^{p_1} \sum_{j=0}^{q_1} u_{ij}$, $v_2 = \sum_{i=q_1+1}^{p_2} \sum_{j=q_1+1}^{q_2} v_{ij}$, $v_{L-1} = \sum_{i=p_{L-2}+1}^{p_{L-1}} \sum_{j=q_{L-2}+1}^{q_{L-1}} v_{ij}$.

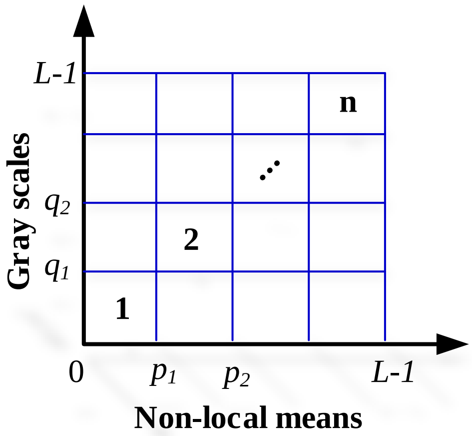

Figure 3. 2D histogram two-dimensional view

where $\{q_1, q_2 \ldots, L-1\}$ and $\{p_1, p_2 \ldots, L-1\}$ shows the gray image scale values and the non-local mean image, respectively. Thus, the threshold set $\{q_1, q, \ldots, q_{n-1}\}$, maximizing $\varphi(p, q)$, shall be used as an optimum threshold by using Kapur's entropy as an objective, and its value means the fitness as follow:

$$f_K(p, q) = argmax\{\varphi(p, q)\} \tag{8}$$

3 Proposed HVSFLA

3.1 Shuffled Frog Leaping Algorithm (SFLA)

Complex problems such as performance evaluation metrics (Zhiang Wu, Li, Cao, & Ge, 2020), optimal performance design (Kordestani, Zhang, Masri, & Shadabfar, 2021), image retrieval (Zenggang, et al., 2019), control cases (Sheng, et al., 2020), and prediction cases (W. Zhou, Lv, Lei, & Yu, 2021) often cannot be solved using exact methods and thus we need to find some approximate solutions instead of exact results. Evolutionary optimization algorithms have strong search ability and optimization performance for complex problems and can solve many real-life optimization problems (F. Yin, et al., 2021). Many new optimization algorithms have been proposed, including slime mould algorithm (SMA) (Li, Chen, Wang, Heidari, & Mirjalili, 2020), Harris hawks optimization (HHO) (Heidari, et al., 2019), Runge Kutta optimizer (RUN) (Ahmadianfar, Asghar Heidari, Gandomi, Chu, & Chen, 2021), hunger games search (HGS) (Y. Yang, Chen, Heidari, & Gandomi, 2021), and colony predation algorithm (CPA) (Jiaze Tu, Chen, Wang, & Gandomi, 2021).

Inspired by the real frog behavior, Eusuf et al. (Eusuff & Lansey, 2003) proposed an algorithm called SFLA in 2003. SFLA has shown effectiveness in tackling real-life applications (Y. Fan, et al., 2021; M. Wang, et al., 2021). The original SFLA has four steps: population initialization, sorting and dividing frogs into memeplexes, exploitation, and knowledge sharing, and shuffling. Initially, in the feature space, a frog solution is randomized and divided into many small groups called memeplexes, depending on the pending goal function regarding fitness values. There are frogs in every memeplex from various backgrounds, and the frogs are manipulated to change the worst position of the frog. In addition, information abstracted from frogs can be shared in each memeplex for shuffling among other memeplexes. The detailed procedure is the following: the frog population is created randomly with equation 9:

$$X_{ij} = lb_i + rand\ (0,1) * (ub_i - lb_i) \tag{9}$$

where *i* means the *ith* frog and the *j* represents the *jth* dimension, and *rand* (0, 1) means the distributed random number in the range of [0, 1]. The fitness of each frog is determined and sorted in descending order, and then the frog population is divided into many memeplexes. The frog is viewed in every memeplex as part of the first memeplex with the highest health benefit. The next one is then going to switch to the second memeplex. In the local search process, the most valuable individuals are frogs with the global best X_{global}, best X_{best} and worst X worst fitness values in any memeplex. The X_{worst} is modified using equation 10:

$$X^* = X_{worst} + Mov_t - Mov_{max} \tag{10}$$

where *t* means generation, Mov_t is the movement of a frog which is calculated by $Mov_t = rand\ (0, 1) * (X_{best} - X_{worst})$, and Mov_{max} means the maximum satisfactory frog drive in the feasible area, if the worst frog position shows consistent growth, the position will be updated; if no changes occur , then equation 9 will be replicated. A frog position will be randomized to replace the worst frog with equation 10. Finally, between two memeplexes, information transfer is carried out, the frogs are sorted and shuffled again to execute the evolution process. The more detailed descriptions can be seen in (Eusuff & Lansey, 2003)

3.2 Horizontal crossover and vertical crossover search

Horizontal crossover search is one of the core steps of the crisscross optimizer (Meng, et al., 2014), and it is motivated by the theory of the Confucius medium and the genetic algorithm. It can significantly enhance the searching capability of optimizers (Y. Liu, et al., 2020). A horizontal crossover search is conducted between two different frogs in each memeplex, allowing different frogs to share knowledge and learn from one another and increase frogs' ability to explore and speed up the algorithm's convergence. A hypothesis is given that the horizontal crossover search is conducted on the nth position vectors of the parent ants x_i and x_j and the calculation can be given as equation 11 and 12.

$$S_i^n = \varepsilon_1 \times x_{in} + (1 - \varepsilon_1) \times x_{jn} + c_1 \times \left(x_{in} - x_{jn}\right) \tag{11}$$

$$S_j^n = \varepsilon_2 \times x_{jn} + (1 - \varepsilon_2) \times x_{in} + c_2 \times \left(x_{jn} - x_{in}\right) \tag{12}$$

$\mathrm{S_i^n}$ and $\mathrm{S_j^n}$are the *n*th position vector ancestors generated by frogs $\mathrm{x_i}$ and $\mathrm{x_j}$, respectively, using the horizontal crossover search, where ε_1 and ε_2 are the random number ranged (0,1) with a uniform distribution, $\mathrm{c_1}$ and $\mathrm{c_2}$ are the random number between (-1,1) with a uniform distribution, $\mathrm{x_{in}}$ is *i*th frog's nth dimension, and $\mathrm{x_{jn}}$ is the *j*th frog's nth dimension.

The vertical crossover search is also one of the core steps of the crisscross optimizer, which may be performed between each memeplex's two separate vectors of positions. It can allow some locally optimal position vectors to continue searching to unchanged as far as possible the usual searching position vectors. Consequently, frogs are always trapped in the local optimum at the later search point due to the stagnation of such position vectors. However, vertical crossover search will enable these position vectors to learn from each other and develop their ability to jump out of local optima effectively.

The vertical crossover search is performed by the vectors *m*th and *n*th of the frogs that can be accomplished by equation 13.

$$S_i^m = \varepsilon \times x_{im} + (1-\varepsilon) \times x_{in} \tag{13}$$

where ε is a random number between reflect (0,1), and S_i^m is the mth a created offspring position vector by vertical crossover search of the vector in mth position and the *n*th position vector of i frog.

3.3 The proposed HVSFLA

To improve performance, the HVSFLA is developed by introducing the horizontal crossover and vertical crossover search mechanisms into the original SFLA algorithm. In the HVSFLA, the algorithm can be broken down into two sections; the first part of the algorithm is the initial steps of SFLA, and the second part is the introduction of the horizontal and vertical crossover search mechanisms. The detailed description of the proposed HVSFLA can be seen in Table 1, where *T* means Maximum iterations, *N* means the population size, *m* is the number of memeplexes, and *n* means the number of individuals in each memeplex.

Table 1 The pseudocode of the HVSFLA

The pseudocode of the HVSFLA
Generate initial population size *N*, calculate the fitness, and maximum iterations *T*;
Divide the population of the frogs into *m* memeplexes in which every memeplex contains *n*; agents *N*=*m***n*;
t=1
while *t*≤*T*
Obtain the global best frog position in the population: X_{global};
Obtain the worst and best frog position in each memeplex:$X_{worst}\ and\ X_{best}$;
for *i*=1: *m*
for j=1:*n*
Generate a new frog position using equation 13: X_j^*;
if f(X_j^*)<f(X_{worst}^i)
$X_{worst}^i = X_j^*$;
endif
endfor
for *k*=1:*n*
Generate a new frog position using equation 11-13: X_k^*;
if f(X_k^*)<f(X_{worst}^i)
$X_{worst}^i = X_k^*$;
endif
endfor
$X_{best}^i = X_{global}$;
endfor

t=t+1;

endwhile

Return X_{global}(Individuals with the best fitness)

4 Numerical results

In this part, several experiments were conducted to evaluate the performance of the proposed HVSFLA. Specifically, the HVSFLA was compared with several competitive evolutionary algorithms using IEEE CEC 2017 benchmark functions. In addition, the impact of the introduced horizontal crossover search and vertical crossover search was also investigated. Notably, the balance and diversity analysis of the proposed HVSFLA and the original SFLA was also carried out strictly. Moreover, the capability of HVSFLA for multi-threshold image segmentation was validated using several Berkeley segmentation datasets 500 (BSDS500), at both the low threshold levels (2, 3, 4, and 5) and the high threshold levels (10, 15, 20, and 25). All experiments were performed on a 2.60GHz Intel® Core 7th generation processor and 16GB RAM computer, and coding was executed by using Matlab 2018b.

4.1 Benchmark function validation

Thirty IEEE CEC 2017 benchmark functions were used, as shown in Table 2. For each case, the search region of each dimension was in the range of [-100, 100]. These functions can be divided into four types: unimodal functions (F1, F2, and F3), multimodal functions (F4 to F10), hybrid functions (F11 to F20), and composition functions (F21 to F30). More details of all test functions can be found in this related article (N. H. Awad, 2016).

In addition, a range of recent algorithms were used for comparison, including grey wolf optimizer (GWO) (Mirjalili, Mirjalili, & Lewis, 2014), Differential Evolution (DE) (R. Storn & K. Price, 1997), whale optimization algorithm (WOA) (Mirjalili & Lewis, 2016), self-adaptive DE (SaDE) (A. K. Qin, Huang, & Suganthan, 2009), the ensemble of mutation strategies and control parameters values for DE (EPSDE) (Mallipeddi, Suganthan, Pan, & Tasgetiren, 2011), comprehensive learning particle swarm optimizer (CLPSO) (J. J. Liang, Qin, Suganthan, & Baskar, 2006), and PSO with an aging leader and challengers (ALCPSO) (W. Chen, et al., 2013). All the algorithms in this experiment were all executed on the same experimental conditions to guarantee the availability and fairness of the experiment as per artificial intelligence rules (S. Feng, Zuo, Zhang, Yin, & Chen, 2021). For this experiment, the population size was set as 40 and the maximum number of evaluations *MaxFE* was set as $4.5*10^5$ and all the algorithms were independently tested thirty times on thirty benchmark functions to reduce the effect of random conditions. The details of parameter settings of all competitive algorithms are listed in Table 3.

Table 2 IEEE CEC 2017 benchmark functions

ID	Name of the function	Class	Search Range	Optimum
F1	*Shifted and Rotated Bent Cigar Function*	*Unimodal*	[-100, 100]	100
F2	*Shifted and Rotated Sum of Different Power Function*	*Unimodal*	[-100, 100]	200
F3	*Shifted and Rotated Zakharov Function*	*Unimodal*	[-100, 100]	300
F4	*Shifted and Rotated Rosenbrock's Function*	*Multimodal*	[-100, 100]	400
F5	*Shifted and Rotated Rastrigin's Function*	*Multimodal*	[-100, 100]	500
F6	*Shifted and Rotated Expanded Scaffer's F6 Function*	*Multimodal*	[-100, 100]	600
F7	*Shifted and Rotated Lunacek Bi-Rastrigin Function*	*Multimodal*	[-100, 100]	700
F8	*Shifted and Rotated Non-Continuous Rastrigin's Function*	*Multimodal*	[-100, 100]	800
F9	*Shifted and Rotated Lévy Function*	*Multimodal*	[-100, 100]	900
F10	*Shifted and Rotated Schwefel's Function*	*Multimodal*	[-100, 100]	1000
F11	*Hybrid Function 1 (N=3)*	*Hybrid*	[-100, 100]	1100
F12	*Hybrid Function 2 (N=3)*	*Hybrid*	[-100, 100]	1200
F13	*Hybrid Function 3 (N=3)*	*Hybrid*	[-100, 100]	1300
F14	*Hybrid Function 4 (N=4)*	*Hybrid*	[-100, 100]	1400
F15	*Hybrid Function 5 (N=4)*	*Hybrid*	[-100, 100]	1500
F16	*Hybrid Function 6 (N=4)*	*Hybrid*	[-100, 100]	1600
F17	*Hybrid Function 6 (N=5)*	*Hybrid*	[-100, 100]	1700
F18	*Hybrid Function 6 (N=5)*	*Hybrid*	[-100, 100]	1800
F19	*Hybrid Function 6 (N=5)*	*Hybrid*	[-100, 100]	1900
F20	*Hybrid Function 6 (N=6)*	*Hybrid*	[-100, 100]	2000
F21	*Composition Function 1 (N=3)*	*Composition*	[-100, 100]	2100
F22	*Composition Function 2 (N=3)*	*Composition*	[-100, 100]	2200
F23	*Composition Function 3 (N=4)*	*Composition*	[-100, 100]	2300
F24	*Composition Function 4 (N=4)*	*Composition*	[-100, 100]	2400
F25	*Composition Function 5 (N=5)*	*Composition*	[-100, 100]	2500
F26	*Composition Function 6 (N=5)*	*Composition*	[-100, 100]	2600
F27	*Composition Function 7 (N=6)*	*Composition*	[-100, 100]	2700
F28	*Composition Function 8 (N=6)*	*Composition*	[-100, 100]	2800
F29	*Composition Function 9 (N=3)*	*Composition*	[-100, 100]	2900
F30	*Composition Function 10 (N=3)*	*Composition*	[-100, 100]	3000

Table 3 Parameter settings of the algorithms compared

Algorithm	Parameters
GWO	a=[2, 0]
WOA	a_1=[2, 0]; a_2=[-2, -1]; b=1
DE	F_{min}=0.2; F_{max}=0.8; CR=0.1
SaDE	F_1=0.9, C_{r1}=0.1; F_2=0.9, C_{r2}=0.9; F_3=0.5, C_{r3}=0.3

	F_4=0.5, C_{r4}=0.3; F_5=0.5, C_{r5}=0.3
EPSDE	$F\in$[0.4, 0.9]; $CR\in$[0.1, 0.9]
CLPSO	$w\in$[0.2, 0.9]; c=1.496
ALCPSO	c_1=c_2=2.0; w=0.4; Θ_0=60; T=2; pro=1/D; Vmax=0.5*search range
HVSFLA	m=5; n=10; α=3; β=5; σ=2

4.2 The impact of horizontal and vertical crossover search

In order to further measure the effectiveness of the diversity control in the HVSFLA and find out the best strategy, the component effect experiments were also carried out on CEC 2017 benchmark functions, where the population size was set as 40, the dimension of optimization cases was set as 30, the maximum number of evaluations *MaxFE* was set as 300000, and each competitive algorithm was executed 30 times independently. In the proposed algorithm, HVSFLA means both horizontal and vertical crossover search operators are introduced into the original SFLA, HSFLA denotes only the horizontal crossover search operator is introduced, and VSFLA indicates only the vertical crossover search operator is introduced. The average ranking of all these algorithms on these CEC 2017 benchmark functions is shown in Table 4. It can be seen that the HVSFLA can achieve the lowest ranking value of 1.46 and thus is ranked first, which implies the combination of both horizontal and vertical crossover search operators is superior to single operator (horizontal or vertical crossover). Therefore, the HVSFLA was used as the experimental algorithm.

Table 4 Average ranking of various mechanism combinations of SFLA

Algorithm	HVSFLA	HSFLA	VSFLA	SFLA
Average ranking	**1.48**	1.88	2.15	3.548

4.3 The balance and diversity analysis

To investigate the diversity and the balance between the diversification and intensification capabilities of the ensemble multi strategy-driven HVSFLA and the original SFLA, the balance and the diversity tests were executed on CEC 2017 test functions. In this part, the population size was set as 40, and the number of the maximum iteration was set as 1000. The balance analysis compared between HVSFLA and the original SFLA is shown in Figure 4, and the diversity analysis convergence graphs are shown in Figure 5.

Regarding the curve lines in Figure 4, the abscissa is the iterations, and the ordinate is the percentage. The blue line and red line indicate the ratio of exploitation (intensification) and the proportion of the exploration (diversification) respectively. Moreover, another metric is an incremental-decremental value that means the intensification and diversification of the algorithm fulfills a state of balance when the value of the exploration and exploitation of the corresponding algorithm is break even. Subsequently, the exploration curve will descend to zero, and the exploitation curve will reach 100%. A reasonable explanation for this phenomenon is that most swarm-based algorithms basically execute the diversification mechanism in the early steps of the algorithm, and at the end of the algorithm, it performs the intensification mechanism to enhance convergence accuracy. It can be observed from Figure 4 that the percentage of the exploitation of HVSFLA is better than that of the conventional SFLA on F1 and F3, which indicates the intensification ability of HVSFLA is strengthened, compared to the original SFLA. Moreover, the percentage of the exploration of HVSFLA is higher than that of the original SFLA on F11 and F20, indicating that the diversification ability of the HVSFLA is also enhanced. Therefore, it can be concluded that the diversification and intensification capabilities of HVSFLA are both improved relative to the basic SFLA due to the introduction of the horizontal and vertical crossover search operators.

Regarding Figure 5, the ordinate indicates the average distance between each frog in the algorithm, the abscissa means the iteration number, the red line is the average distance of the HVSFLA, and the blue curve means the average distance of the original SFLA, which reflects the individual distribution and the diversity of the population. It can be seen from this figure that the average distance between the frogs is bigger because frog positions were generated randomly in the initialization phase. The curve is descending as the iterations increase and stabilizes in the end. On these selected functions, the trend of the proposed HVSFLA appears to stabilize much earlier than the original SFLA, indicating that the introduced two search operators enhance the diversification and intensification capabilities of HVSFLA. It should be noted that the curves of HVSFLA can still perform modifications slightly when it has arrived at a stable state because the vertical crossover search operator can improve the diversification of HVSFLA. Therefore, the diversification and intensification capabilities of the proposed HVSFLA are significantly improved.

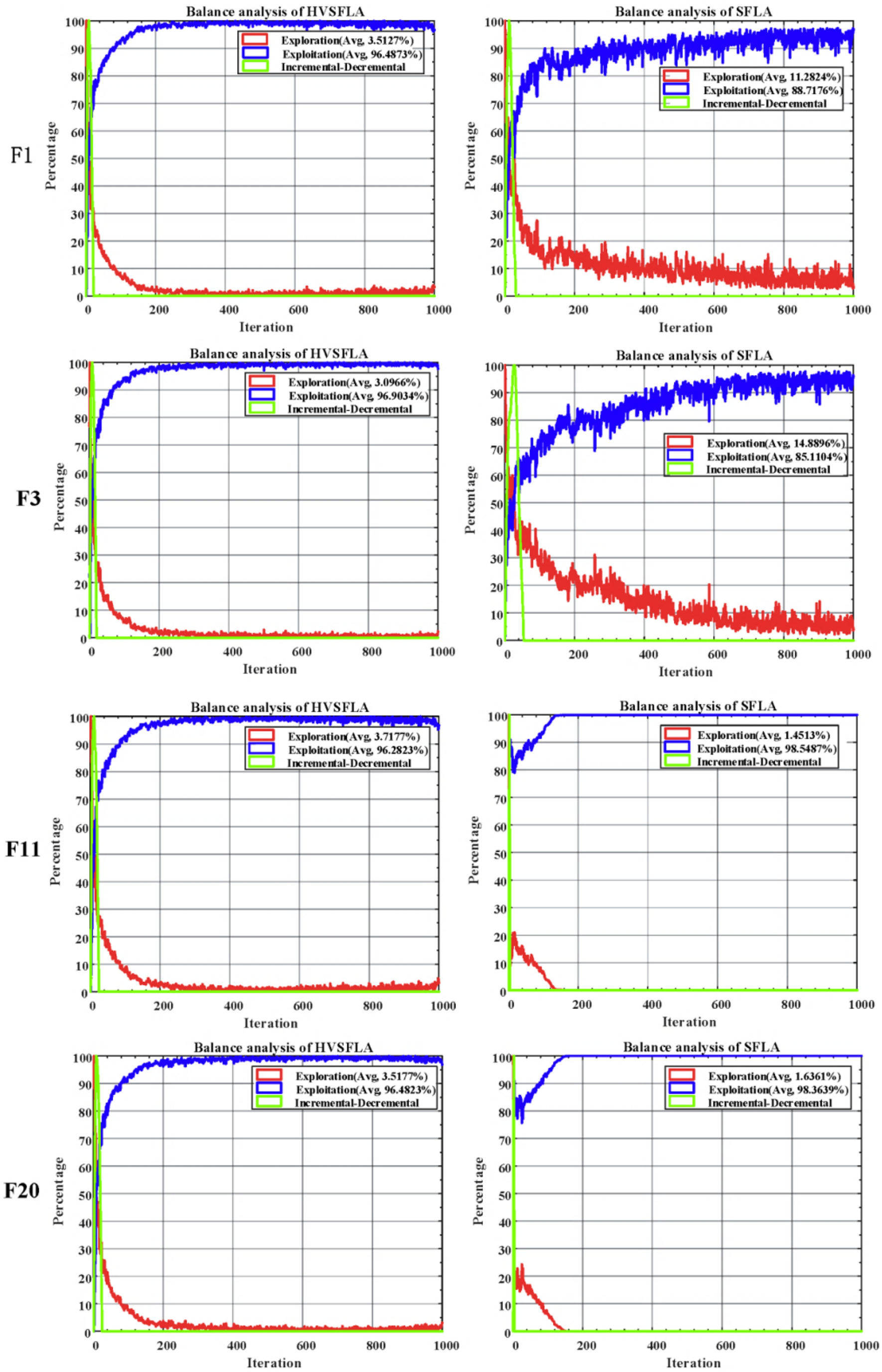

Figure 4. The balance analysis plots of F1, F3, F11, F20

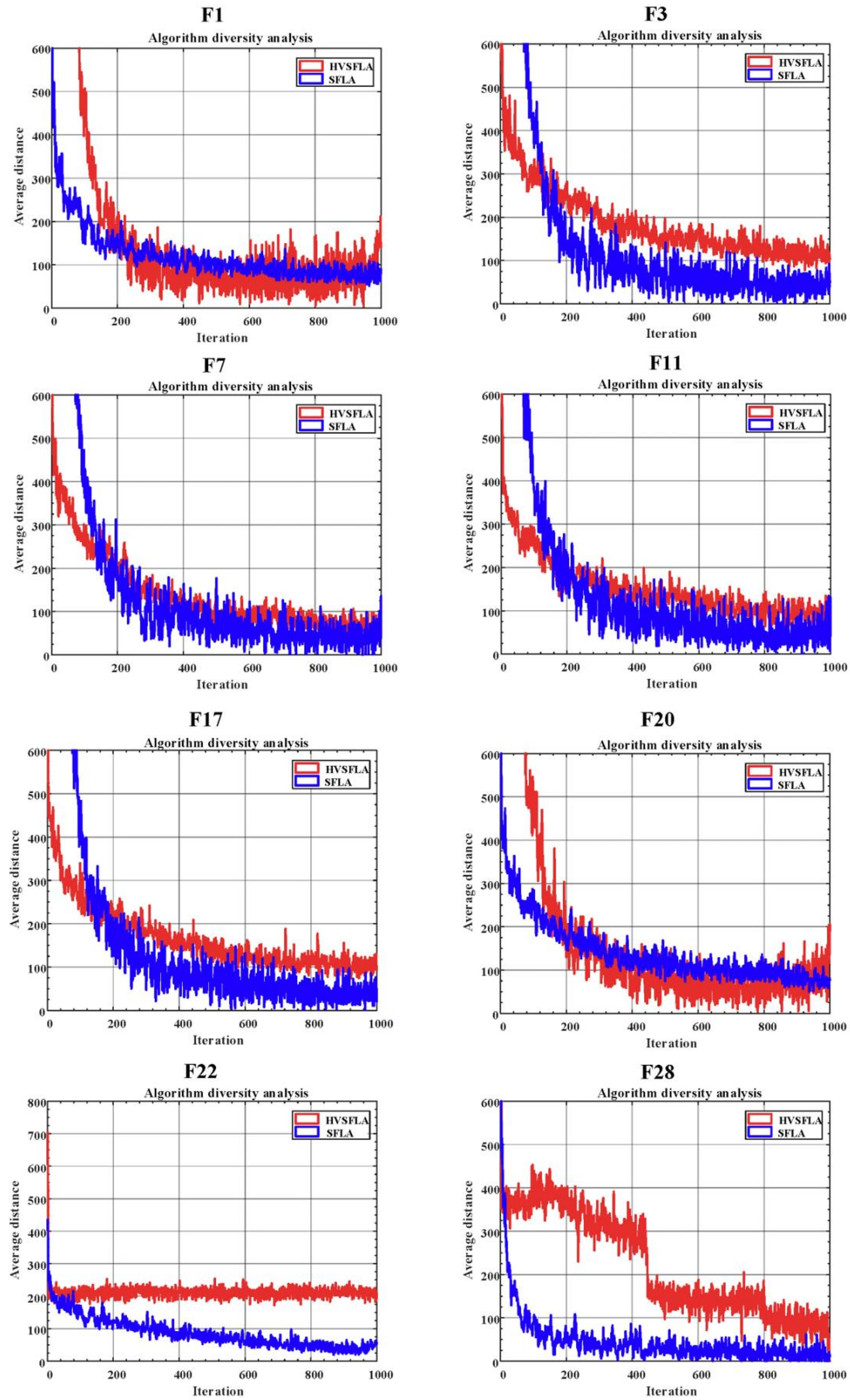

Figure 5. The diversity analysis plots of F1, F3, F7, F11, F17, F20, F22, F28

4.4 The results on the benchmark functions

In this subsection, to evaluate its performance, the proposed HVSFLA was compared with several competitive evolutionary algorithms using 30 IEEE CEC 2017 benchmark functions. The metrics mean value (*mean*) and standard deviation value (*std*) were both used in this test, and each algorithm was executed 30 times independently for each test function. The statistical results of algorithms are presented in Table 5. In Table 5, the last row indicates that comparison results between HVSFLA and other competitors, and the best *mean* and *std* value are marked in bold, where " + ", " − ", and " = " means that the result is significantly better, significantly worse, and statistically similar to that obtained by HVSFLA, respectively.

It can be seen from Table 5 that the proposed HVSFLA significantly outperforms the original SFLA and other competitors on most of the test problems, and it also obtains the theoretical optimal values on F1, F2, F3, F6, and F9. besides the CLPSO, EPSDE, SaDE, and DE all acquire the theoretical optimal solution on F6 case. The detailed analysis can be summarized as follows: the proposed HVSFLA outperforms the original SFLA, ALCPSO, and WOA on all thirty functions; HVSFLA performs better than CLPSO on twenty-five functions and is worse than CLPSO on one function, it shows a tie on the other four test functions. HVSFLA shows better performance than EPSDE on twenty-three functions; it performs similarly to EPSDE on two functions and is worse than EPSDE on five test functions; HVSFLA does better on twenty-two functions than SaDE, is inferior to SaDE on six test functions and performs similarly on two functions; HVSFLA is superior to GWO on twenty-nine functions and performs worse only on one function; HVSFLA also has better performance than DE on twenty-nine functions, it shows a tie with DE on only one function. Notably, on a few test functions such as F8, the standard deviation of HVSFLA is worse than that of some other algorithms. One of the potential reasons may be that the introduction of multi-strategies results in impaired stability, indicating that there is still room for improvement in the stability of the HVSFLA.

It should be noted that these deficiencies are very small and maybe negligible in practical problems; after all, the total average search capability of the HVSFLA is still very meaningful in practical problems. In addition, the convergence curves of HVSFLA versus other competitive algorithms on several functions are shown in Figure 6. As far as each function is concerned, the HVSFLA shows an outstanding search capability. As shown on the vertical axis of the F12, it shows rapid convergence in the initial stage of optimization until the final convergence. As can be observed from Figure 6, the proposed HVSFLA also shows the best convergence capability among all these algorithms. Based on the above analysis, it can be concluded that HVSFLA is significantly superior in performance to the original SFLA and other peers due to the introduced horizontal and vertical crossover search operators. Horizontal crossover search enables different frogs to exchange information, which can guarantee the effective exploration of each frog and speed up the convergence rate. Meanwhile, vertical crossover search can make frogs in stagnation continue to search actively. With the introduction of these two operators, a better balance between diversification and intensification can be ensured, rendering it a potential technology for image segmentation tasks.

Table 5 Statistical results evaluated by different algorithms for IEEE CEC 2017

Function		HVSFLA	SFLA	CLPSO	ALCPSO	EPSDE	SaDE	GWO	WOA	DE
F_1	mean	**1.0000E+02**	4.3166E+09	1.3215E+02	5.0153E+03	1.0002E+02	2.6325E+03	2.0326E+09	2.1685E+06	9.7865E+02
	std	**1.1568E-02**	2.0368E+09	3.1982E+01	6.5298E+03	9.2856E-11	2.4126E+03	1.7563E+09	1.4852E+06	9.5963E+02
F_2	mean	**2.0000E+02**	1.1658E+34	4.4850E+15	5.2637E+16	5.1258E+15	2.0261E+10	3.3251E+30	1.2638E+20	1.8924E+22
	std	**5.0324E-06**	4.2638E+34	1.8563E+16	2.1569E+17	2.0621E+16	7.4126E+10	1.8026E+31	5.4026E+20	4.1257E+22
F_3	mean	**3.0000E+02**	6.5368E+04	1.4128E+04	2.9320E+04	1.7029E+04	3.0105E+02	3.3620E+04	1.6659E+05	3.3015E+04
	std	**1.4732E-08**	8.50231E+03	3.38264E+03	4.3920E+03	7.7541E+04	2.5369E-01	1.1258E+04	7.9239E+04	5.4128E+03
F_4	mean	4.1879E+02	1.1853E+03	4.7213E+02	5.0359E+02	**4.0456E+02**	4.3526E+02	5.8462E+02	5.4521E+02	4.9126E+02
	std	2.7230E+01	3.3856E+02	1.7302E+01	2.1325E+01	**3.2438E+00**	3.7208E+01	8.0125E+01	3.4503E+01	8.2432E+00
F_5	mean	**5.3524E+02**	7.45632E+02	5.4805E+02	5.9236E+02	5.3986E+02	5.4326E+02	6.0753E+02	8.0523E+02	6.1056E+02
	std	**7.1035E+00**	5.10235E+01	6.5326E+00	3.2015E+01	7.2354E+00	1.0853E+01	3.1936E+01	7.8290E+01	8.2906E+00
F_6	mean	6.0000E+02	6.5823E+02	6.0000E+02	6.0523E+02	**6.0000E+02**	6.0000E+02	6.0785E+02	6.7203E+02	6.0000E+02
	std	5.4032E-13	1.4502E+01	8.2032E-12	2.9852E+00	**0.0000E+00**	1.5639E-05	3.3652E+00	1.1209E+01	2.1025E-14
F_7	mean	7.7523E+02	1.0325E+03	7.8639E+02	8.4402E+02	7.7315E+02	**7.6725E+02**	8.6653E+02	1.2365E+03	8.4520E+02
	std	1.1685E+01	9.1289E+01	8.3421E+00	3.5421E+01	8.2985E+00	**9.6235E+00**	3.7854E+01	8.4756E+01	9.4218E+00
F_8	mean	**8.4125E+02**	1.0236E+03	8.6025E+02	9.0302E+02	8.4596E+02	8.4213E+02	8.7632E+02	1.0063E+03	9.1216E+02
	std	**1.0128E+01**	3.5436E+01	6.6785E+00	3.9852E+01	1.1632E+01	9.7806E+00	1.6852E+01	4.9852E+01	9.5821E+00
F_9	mean	**9.0000E+02**	5.4123E+03	9.2001E+02	1.6832E+03	9.0043E+02	9.0504E+02	1.6325E+03	7.7852E+03	9.0025E+02
	std	**3.6533E-14**	1.8632E+03	1.4215E+01	7.0752E+02	8.7126E-01	7.7578E+00	5.0412E+02	3.0125E+03	3.7585E-13
F_{10}	mean	3.7325E+03	6.1958E+03	**3.5561E+03**	4.2148E+03	4.6458E+03	3.6325E+03	3.9289E+03	5.9885E+03	5.9958E+03
	std	5.0452E+02	6.2352E+02	**3.0622E+02**	6.8700E+02	4.2651E+02	7.6148E+02	6.0802E+02	7.7854E+02	2.5245E+02

F_{11}	mean	**1.1124E+03**	2.3889E+03	1.16356E+03	1.2887E+03	1.1325E+03	1.1789E+03	1.6544E+03	1.5102E+03	1.1626E+03
	std	**2.5603E+01**	5.57851E+02	1.9548E+01	6.0456E+01	1.5254E+01	3.2231E+01	6.2912E+02	1.1601E+02	2.0432E+01
F_{12}	mean	1.7582E+04	3.0325E+08	4.5954E+05	3.1269E+05	5.4702E+04	1.8321E+04	3.2520E+07	4.2241E+07	2.1985E+06
	std	**8.5241E+03**	2.7328E+08	2.3652E+05	5.2215E+05	7.1752E+04	9.8635E+03	4.0452E+07	2.8962E+07	1.1321E+06
F_{13}	mean	1.9126E+03	1.1285E+05	**1.7542E+03**	2.8051E+04	7.1952E+03	9.9201E+03	3.3687E+06	1.6125E+05	5.4852E+04
	std	1.6128E+03	6.2312E+04	**3.3852E+02**	2.3102E+04	1.3256E+04	5.1623E+03	1.3742E+07	1.1482E+05	2.7201E+04
F_{14}	mean	1.4885E+03	5.4132E+05	3.1132E+04	2.4543E+04	1.5041E+03	**1.4865E+03**	2.1285E+05	9.3653E+05	5.7632E+04
	std	4.7242E+01	6.0976E+05	2.5670E+04	4.2870E+04	9.9529E+01	**5.7324E+01**	3.6570E+05	9.7476E+05	3.1215E+04
F_{15}	mean	**1.5412E+03**	2.8369E+04	1.6541E+03	1.5536E+04	1.6332E+03	1.9855E+03	1.4215E+06	7.6885E+04	1.0985E+04
	std	**2.9012E+01**	1.8524E+04	7.9852E+01	1.5591E+04	1.3051E+02	5.5232E+02	6.1721E+06	5.5609E+04	5.0425E+03
F_{16}	mean	**1.9000E+03**	3.2332E+03	2.1005E+03	2.5421E+03	2.1863E+03	2.0401E+03	2.3902E+03	3.5169E+03	2.0963E+03
	std	**2.1256E+02**	3.7365E+02	1.3668E+02	3.0482E+02	1.8662E+02	1.6302E+02	2.3080E+02	4.2632E+02	1.4836E+02
F_{17}	mean	1.7950E+03	2.4926E+03	1.8088E+03	2.1626E+03	1.8921E+03	1.7352E+03	1.9952E+03	2.5362E+03	1.8436E+03
	std	6.5541E+01	2.5826E+02	4.5650E+01	2.0582E+02	7.3336E+01	4.7882E+01	1.4149E+02	2.6854E+02	3.6741E+01
F_{18}	mean	**5.9014E+03**	4.1562E+06	1.4878E+05	2.6523E+05	**5.9029E+03**	1.2632E+04	1.0325E+06	2.1256E+06	3.3123E+05
	std	**2.3254E+03**	4.6623E+06	9.6654E+04	2.9201E+05	**6.3852E+03**	8.4521E+03	1.6632E+06	2.2362E+06	1.6963E+05
F_{19}	mean	**1.9432E+03**	9.3517E+06	1.9700E+03	1.2920E+04	1.9455E+03	2.2758E+03	1.8856E+06	2.1328E+06	9.8752E+03
	std	**1.2560E+02**	7.4200E+06	6.2198E+01	1.3780E+04	3.7223E+01	1.4050E+03	5.6856E+06	1.9169E+06	6.3852E+03
F_{20}	mean	2.1035E+03	2.6652E+03	2.1852E+03	2.3588E+03	2.1251E+03	**2.0766E+03**	2.3655E+03	2.7159E+03	2.1145E+03
	std	6.6421E+01	2.1685E+02	7.3235E+01	1.8741E+02	7.2582E+01	**6.3526E+01**	1.1565E+02	2.0248E+02	5.4542E+01
F_{21}	mean	2.3425E+03	2.4836E+03	**2.3312E+03**	2.4044E+03	2.3421E+03	2.3402E+03	2.3742E+03	2.5782E+03	2.4225E+03
	std	8.1632E+00	4.4785E+01	**5.1598E+01**	3.0160E+01	6.7185E+00	8.5620E+00	1.8354E+01	5.3905E+01	9.3365E+00

F_{22}	mean	**2.3000E+03**	3.4692E+03	2.3329E+03	4.0930E+03	5.6092E+03	2.3125E+03	4.3332E+03	7.3885E+03	3.3712E+03
	std	**1.1063E-12**	1.2970E+03	1.6221E+01	1.8106E+03	1.4532E+03	1.0621E+00	1.4249E+03	1.2632E+03	1.4632E+03
F_{23}	mean	**2.6885E+03**	2.8985E+03	2.7052E+03	2.7952E+03	2.6963E+03	2.6908E+03	2.7582E+03	3.0594E+03	2.7654E+03
	std	**1.1142E+01**	6.1305E+01	7.6085E+00	3.7352E+01	8.8669E+00	1.0685E+01	3.0820E+01	1.0592E+02	8.0236E+00
F_{24}	mean	**2.8625E+03**	2.9956E+03	2.8885E+03	2.9952E+03	2.8658E+03	2.8586E+03	2.9275E+03	3.1725E+03	2.9752E+03
	std	**1.4623E+01**	3.0468E+01	1.1790E+02	6.3805E+01	7.1936E+00	1.6854E+01	4.5362E+01	7.7690E+01	9.5470E+00
F_{25}	mean	2.8958E+03	3.2452E+03	2.8952E+03	2.8920E+03	**2.8782E+03**	2.8909E+03	2.9790E+03	2.9462E+03	2.8882E+03
	std	1.1985E+00	7.9236E+01	6.6025E-01	1.5742E+01	**6.4426E+00**	9.4852E+00	3.2368E+01	2.6985E+01	3.8852E-01
F_{26}	mean	3.8523E+03	6.1582E+03	**3.5521E+03**	4.8885E+03	3.8220E+03	3.7526E+03	4.6240E+03	7.5522E+03	4.7235E+03
	std	1.7521E+02	1.1075E+03	**5.0632E+02**	4.1852E+02	1.8386E+02	6.1852E+02	3.7256E+02	9.6929E+02	9.2806E+01
F_{27}	mean	**3.1852E+03**	3.3523E+03	3.2235E+03	3.2563E+03	3.2023E+03	3.2321E+03	3.2420E+03	3.3690E+03	3.2025E+03
	std	**6.7230E+00**	6.0121E+01	3.3425E+00	2.7562E+01	1.2425E-04	1.1620E+01	2.3946E+01	7.3956E+01	2.8126E+00
F_{28}	mean	**3.1276E+03**	3.7923E+03	3.2362E+03	3.2362E+03	3.3021E+03	3.1280E+03	3.3852E+03	3.3362E+03	3.2023E+03
	std	**4.7652E+01**	1.9384E+02	1.0788E+01	3.7921E+01	1.1652E-04	5.2250E+01	5.4752E+01	1.9805E+01	3.8120E+01
F_{29}	mean	3.3825E+03	4.7520E+03	3.4726E+03	3.7632E+03	3.3852E+03	**3.3420E+03**	3.7099E+03	4.7021E+03	3.5602E+03
	std	5.8200E+01	4.6425E+02	7.2825E+01	1.6452E+02	1.0660E+02	**3.3352E+01**	1.7108E+02	4.0542E+02	7.2321E+01
F_{30}	mean	5.9623E+03	3.5852E+07	9.0988E+03	1.5463E+04	**3.2251E+03**	6.4926E+03	6.2325E+06	1.0521E+07	1.4895E+04
	std	7.7912E+02	3.4220E+07	1.6345E+03	6.3355E+03	**5.6321E+01**	1.2030E+03	5.9885E+06	8.3256E+06	4.1852E+03
+/=/-		NA	30/0/0	25/1/4	30/0/0	23/2/5	22/2/6	29/0/1	30/0/0	29/1/0

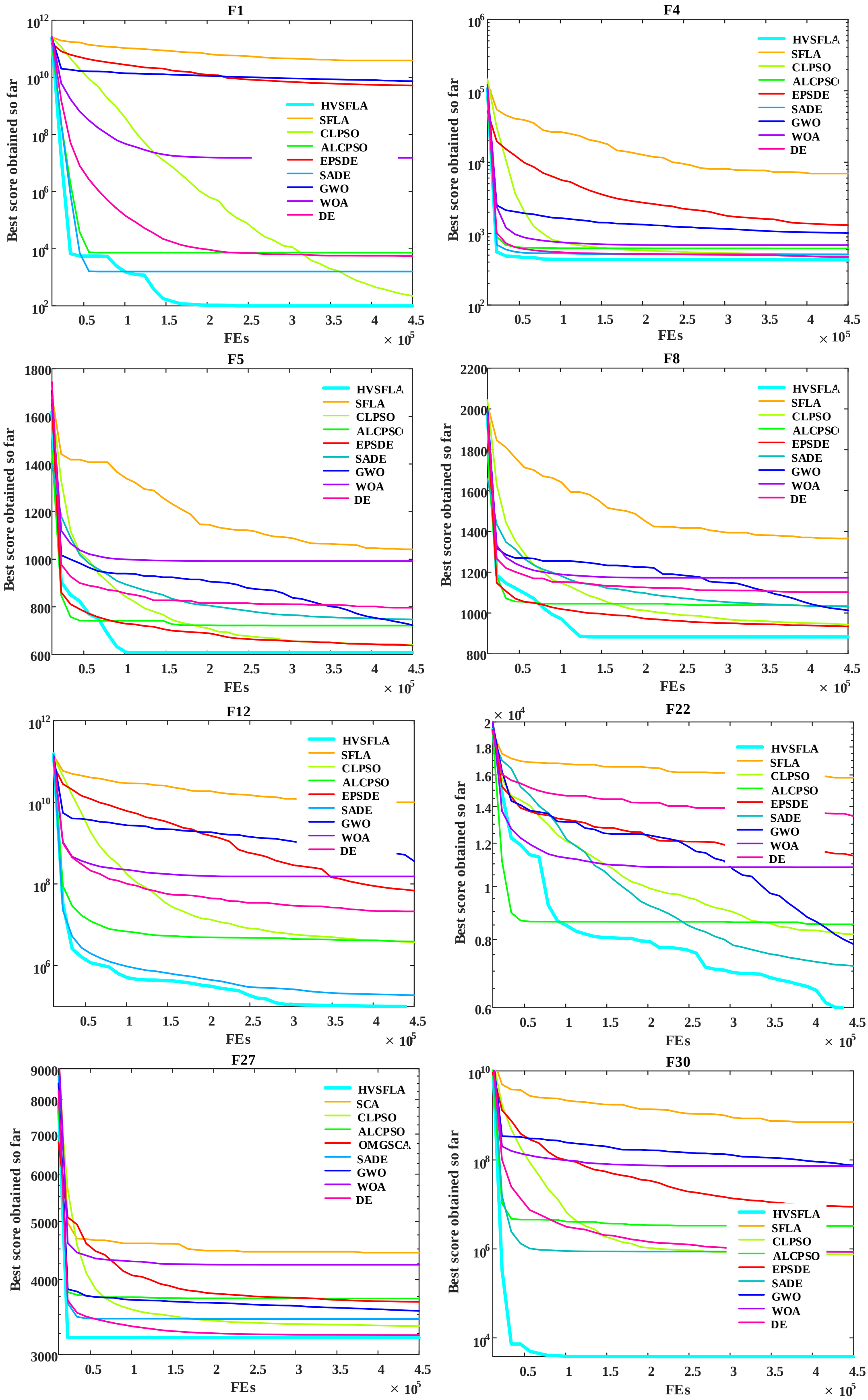

Figure 6. The convergence curves of selected functions

4.5 Experiments on MTIS

In this subsection, the capability of the proposed HVSFLA in multi-threshold image segmentation was investigated thoroughly. To measure its performance, HVSFLA was compared with eight other algorithms, including extended ant colony optimization (ACOR) (Socha & Dorigo, 2008), WOA (Mirjalili & Lewis, 2016), DE (R. Storn & K. J. J. o. G. O. Price, 1997), bat-inspired algorithm (BA) (X.-S. Yang, 2010), PSO (Kennedy & Eberhart, 1995), a hybrid particle swarm optimization algorithm (CGPSO) (Jia, Zheng, Qu, & Khan, 2011), enhanced grey wolf optimization strategy (IGWO) (Cai, et al., 2019), and enhanced Moth-flame optimizer with mutation strategy (LGCMFO) (Xu, et al., 2019). Furthermore, both the low threshold levels (2, 3, 4, and 5) and high threshold levels (from 10 to 25) with five tolerances of the arithmetic were used to evaluate the performance of the proposed algorithm. In addition, according to work in (D. Zhao, Liu, Yu, Heidari, Wang, Oliva, et al., 2021), three other metrics, i.e., PSNR, SSIM, and FSIM, were also used to measure the results of image segmentation .

4.5.1 Experiment design and arrangement

In this subsection, images 12003, 38082, 19021, 65010, 35010, and 113016 abstracted from Berkeley segmentation dataset 500 were used for MTIS, and all these images are the most commonly used images to evaluate segmentation algorithms. Notably, the potential structure of these images is referenced with the images of breast invasive ductal carcinoma that will be explored in this study—figure 7 shows these original images and non-local means 2D histograms. For a fair comparison, the HVSFLA and other competitive algorithms were all executed under the same situation. The size of the population was set as 40, the number of iterations was set as 100, image size was 481×321, and all algorithms were carried out 30 times individually. In addition, the performance was evaluated at various threshold levels of each algorithm, including the low threshold levels of 2, 3, 4, 5, and the high threshold levels from 10 to 25 with five tolerances of the arithmetic.

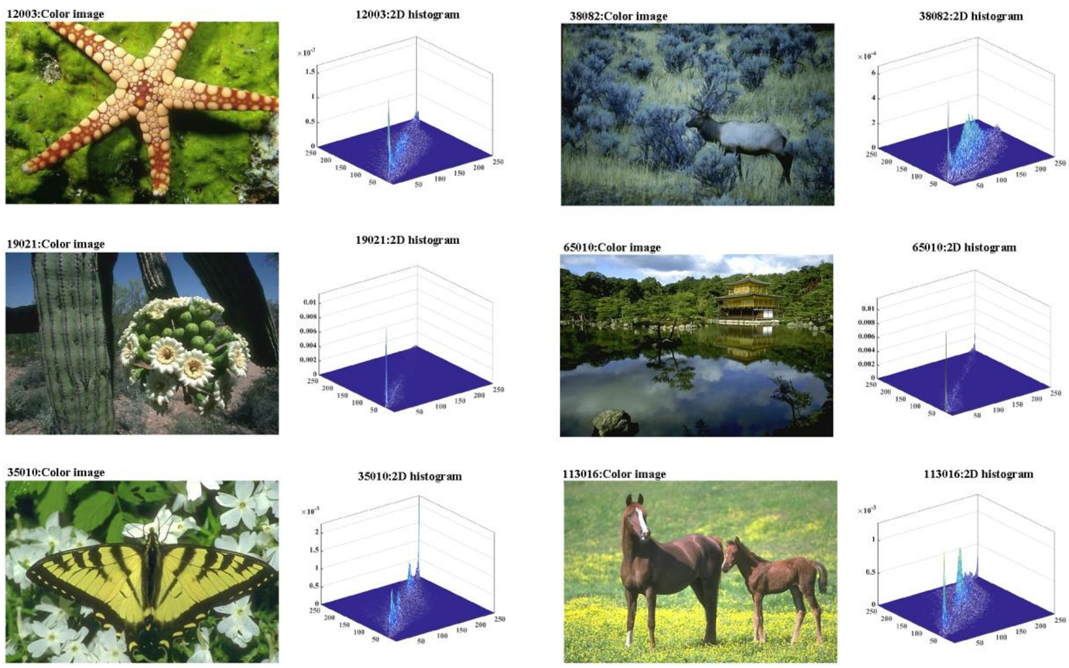

Figure 7. Samples of the segmented images.

4.5.2 Performance evaluation parameters

In this study, three metrics, i.e., PSNR, SSIM, and FSIM, were used to evaluate image segmentation results. Since these three metrics are effective in evaluating the performance of segmentation algorithms in the field of image segmentation, we used them as per work (D. Zhao, Liu, Yu, Heidari, Wang, Oliva, et al., 2021). The greater the PSNR value, the better performance of the segmentation algorithm, and the PSNR equation is defined (12). SSIM can calculate the resemblance between two images and describes it as equation 18; the higher its value, the greater the threshold segmentation effect is; the equations of PSNR and SSIM are as follows:

$$PSNR = 20 \cdot \log_{10}\left(\frac{255}{RMSE}\right) \tag{14}$$

$$RMSE = \sqrt{\frac{\sum_{i=0}^{M-1}\sum_{j=0}^{N-1}\left(I_{ij}-Seg_{ij}\right)^2}{M \times N}} \tag{15}$$

$$SSIM = \frac{(2\mu_I\mu_{Seg}+c_1)(2\sigma_{I,Seg}+c_2)}{(\mu_I{}^2+\mu_{Seg}{}^2+c_1)(\sigma_I{}^2+\sigma_{Seg}{}^2+c_2)} \tag{16}$$

FSIM refers to the feature similarity of the original image to the split image and is based on two features: high phase recombination and gradient amplitude, which are used to determine the local structure and provide contrast information. The value of FSIM belongs to [0, 1]; the closer the value is to 1, the better performance of the segmentation algorithm. Its equation is as follows:

$$FSIM = \frac{\sum_{I\in\Omega} S_L(X)PC_m(X)}{\sum_{I\in\Omega} PC_m(X)} \tag{17}$$

$$S_L(X) = S_{PC}(X)S_G(X) \tag{18}$$

$$S_{PC}(X) = \frac{2PC_1(X)PC_2(X)+T_1}{PC_1^2(X)PC_2^2(X)+T_1} \tag{19}$$

$$S_G(X) = \frac{2G_1(X)G_2(X)+T_2}{G_1^2(X)G_2^2(X)+T_2} \tag{20}$$

$$G = \sqrt{G_x^2 + G_y^2} \tag{21}$$

$$PC(X) = \frac{E(X)}{(\varepsilon+\sum_m A_n(X))} \tag{22}$$

A more detailed description of these three metrics can be seen in (D. Zhao, Liu, Yu, Heidari, & Chen, 2020), and it should be noted that the mean, variance, and Wilcoxon signed-rank tests were all used to further evaluate PSNR, SSIM, and FSIM test data.

4.5.3 Low-threshold experimental study

This subsection assesses HVSFLA's picture segmentation capability at low threshold levels (2, 3, 4, and 5), and images 12003, 38082, 19021, 65010, 35010, and 113016 were used. The proposed HVSFLA was compared with several other algorithms including ACOR (Socha & Dorigo, 2008), WOA (Mirjalili & Lewis, 2016), DE (R. Storn & K. J. J. o. G. O. Price, 1997), BA (X.-S. Yang, 2010), PSO (Kennedy & Eberhart, 1995), CGPSO (Jia, et al., 2011), IGWO (Cai, et al., 2019), and LGCMFO (Xu, et al., 2019). PSNR, SSIM, and FSIM were used to analyze the results, and the mean, variance, and the Wilcoxon signed-rank test were also used to further analyze the segmentation results. The AVG and STD of the results of PSNR, SSIM, and FSIM are listed in Table 6, 7, and 8 respectively, and the results of further analysis are also shown in Table 9 and 10, where the mean value of the overall ranking is the Mean, Rank shows the level ranking, symbols "+","=", "-", mean that the performance of HVSFLA is better than the comparison algorithms, equal to the comparison algorithms and worse than the comparison algorithms, respectively. It can be seen from these Tables that the mean value of the overall ranking of HVSFLA has the smallest values. According to the Wilcoxon signed-rank test, the proposed HVSFLA is significantly superior to other algorithms at low threshold levels.

Table 6 The comparison results of PSNR at low threshold levels

Thresholds		HVSFLA	ACOR	WOA	DE	BA	PSO	CGPSO	IGWO	LGCMFO
2	+/−/=	~	4/1/1	3/0/3	3/0/3	4/0/2	4/0/2	3/0/3	4/0/2	4/0/2
	Mean	**1.7256**	3.0369	6.5587	5.1652	7.0258	5.1785	5.6325	8.1562	6.5452
	Rank	**1**	2	7	3	8	4	5	9	6
3	+/−/=	~	5/0/1	3/0/3	2/0/4	3/0/3	2/0/4	2/1/3	5/0/1	3/1/2
	Mean	**3.1562**	3.3365	7.3258	6.0652	6.8325	4.3425	4.1632	7.6685	6.1521
	Rank	**1**	2	8	5	7	4	3	9	6

	+/−/=	~	4/0/2	5/0/1	2/1/3	3/0/3	3/0/3	2/2/2	5/0/1	3/0/3
4	Mean	**3.1521**	3.6698	9.0365	4.6754	6.6652	4.0256	3.3635	8.8369	5.8542
	Rank	**1**	3	9	5	7	4	2	8	6
	+/−/=	~	2/0/4	4/0/2	3/0/3	5/0/1	4/0/2	4/0/2	3/0/3	3/1/2
5	Mean	**2.8231**	4.0125	8.3521	4.5210	7.6352	3.5520	3.5026	8.8362	5.1562
	Rank	**1**	4	8	5	7	3	2	9	6

Table 7 The comparison results of SSIM at low threshold levels

Thresholds		HVSFLA	ACOR	WOA	DE	BA	PSO	CGPSO	IGWO	LGCMFO
	+/−/=	~	4/0/2	3/0/3	4/0/2	3/1/2	5/0/1	3/0/3	5/0/1	4/1/1
2	Mean	**1.7852**	3.0563	6.5258	5.1785	7.0632	5.1569	5.6362	8.1452	6.5263
	Rank	**1**	2	6	4	8	3	5	9	7
	+/−/=	~	3/0/3	4/0/2	2/1/3	4/1/1	4/0/2	3/0/3	5/1/0	4/1/1
3	Mean	**3.1529**	3.3362	7.3362	6.0524	6.8687	4.3635	4.1652	7.6152	6.1632
	Rank	**1**	2	8	5	7	4	3	9	6
	+/−/=	~	3/0/3	5/0/1	3/1/2	3/0/3	2/2/2	4/1/1	5/0/1	4/0/2
4	Mean	**3.1956**	3.6639	9.0698	4.6658	6.6754	4.0321	3.3587	8.8412	5.8654
	Rank	**1**	3	9	5	7	4	2	8	6
	+/−/=	~	4/0/2	4/1/1	3/0/3	4/0/2	3/0/3	3/1/2	3/0/3	3/0/3
5	Mean	**2.8452**	4.0362	8.3562	4.5695	7.6542	3.5652	3.5214	8.8325	5.1521
	Rank	**1**	4	8	5	7	3	2	9	6

Table 8 The comparison results of FSIM at low threshold levels

Thresholds		HVSFLA	ACOR	WOA	DE	BA	PSO	CGPSO	IGWO	LGCMFO
	+/−/=	~	3/0/3	3/0/3	3/2/1	4/1/1	3/0/3	3/0/3	5/0/1	5/0/1
2	Mean	**1.7425**	3.0365	6.5251	5.1562	7.0652	5.1452	5.6956	8.1235	6.5421
	Rank	**1**	2	6	4	8	3	5	9	7
	+/−/=	~	2/0/4	3/0/3	4/0/2	3/0/3	3/1/2	4/1/1	5/0/1	3/1/2
3	Mean	**3.1524**	3.3635	7.3452	6.0397	6.8675	4.3452	4.1398	7.6635	6.1452
	Rank	**1**	2	8	5	7	4	3	9	6
	+/−/=	~	4/0/2	5/0/1	3/1/2	2/0/4	3/1/2	4/1/1	5/0/1	3/0/3
4	Mean	**3.2352**	3.6524	9.0251	4.6365	6.6452	4.0254	3.3362	8.8452	5.8521
	Rank	**1**	3	10	5	8	4	2	8	6
	+/−/=	~	3/0/3	3/0/3	2/1/3	4/0/2	4/1/1	2/2/2	3/0/3	3/1/2
5	Mean	**2.7521**	4.0362	8.3251	4.5985	7.6632	3.5632	3.5125	8.8521	5.1652
	Rank	**1**	4	8	5	7	3	2	9	6

Table 9 displays the highest entropy values of Kapur reached by low-threshold segmentation algorithms; the number of iterations for the optimum threshold is shown in Table 10. In terms of fitness, it can be seen from Table 9 that the proposed HVSFLA has obvious advantages in finding the highest entropy of Kapur relative to other competitive algorithms for low-threshold imaging experiments. Regarding the number of iterations, it can be seen from Table 10 that the proposed HVSFLA can most easily reach the desired threshold, which also means that its convergence is also the fastest at low threshold levels. Figure 8 presents the segmentation results of the proposed HVSFLA and other peers on the segmentation of the image 12003 at threshold level5. It can be seen that HVSFLA outperforms competitive algorithms in terms of detail retention of the original image and segmentation effect. In addition, the p-values of the HVSFLA compared to other algorithms at low threshold levels obtained by the Wilcoxon test are shown in Table 11, and it can be seen that most of the values are less than 0.05, indicating that the proposed HVSFLA is significantly different from other algorithms in terms of statistics at low threshold levels.

Based on the above analyses, the HVSFLA demonstrated important advanced image information preservation and overall effect relative to other algorithms and can run faster than other algorithms to reach the ideal threshold to find Kapur's entropy. Therefore, it can be concluded that the method HVSFLA has great potential for image segmentation at low threshold levels.

Table 9 The fitness value results at low threshold levels

Image	Thresholds	HVSFLA	ACOR	WOA	DE	BA	PSO	CGPSO	IGWO	LGCMFO
12003	2	**2.5432E+01**	2.4523E+01	2.4325E+01	2.4752E+01	2.4746E+01	2.4598E+01	2.2654E+01	2.4312E+01	2.4577E+01
	3	**3.1852E+01**	3.1215E+01	3.1562E+01	3.1421E+01	3.1436E+01	3.1695E+01	2.8254E+01	3.125E+01	3.1523E+01
	4	**3.8956E+01**	3.6325E+01	3.6852E+01	3.6325E+01	3.6987E+01	3.70852E+01	3.7365E+01	3.7652E+01	3.7662E+01
	5	4.3562E+01	4.3025E+01	4.3236E+01	4.2041E+01	4.3526E+01	4.3125E+01	3.9423E+01	4.3252E+01	**4.6563E+01**
38082	2	**2.7589E+01**	2.6215E+01	2.6126E+01	2.6125E+01	2.6125E+01	2.4256E+01	2.6125E+01	2.6126E+01	2.6125E+01
	3	**3.4526E+01**	3.2354E+01	3.2542E+01	3.2362E+01	3.2526E+01	3.2325E+01	3.2546E+01	3.2256E+01	3.2263E+01
	4	**3.9899E+01**	3.8362E+01	3.8632E+01	3.8325E+01	3.8362E+01	3.8362E+01	3.8452E+01	3.8326E+01	3.8362E+01
	5	**4.5821E+01**	4.3852E+01	4.3215E+01	4.3602E+01	4.3425E+01	4.3758E+01	4.3024E+01	4.3523E+01	4.3452E+01
19021	2	**2.8526E+01**	2.6325E+01	2.0524E+01	2.0215E+01	2.1253E+01	2.2654E+01	2.1526E+01	2.1895E+01	2.1256E+01
	3	**2.7526E+01**	2.6523E+01	2.6366E+01	2.6852E+01	2.5632E+01	2.5698E+01	2.6652E+01	2.6562E+01	2.6236E+01
	4	3.2635E+01	3.3056E+01	3.1852E+01	3.2103E+01	**3.4326E+01**	3.2063E+01	3.2082E+01	3.2631E+01	3.213E+01
	5	**3.9856E+01**	3.7012E+01	3.7012E+01	3.7145E+01	3.7523E+01	3.5632E+01	3.6598E+01	3.6523E+01	3.3625E+01
65010	2	**2.4698E+01**	2.3623E+01	2.3523E+01	2.374E+01	2.3523E+01	2.3563E+01	2.3321E+01	2.3563E+01	2.3200E+01
	3	**2.9989E+01**	2.9852E+01	2.9821E+01	2.9852E+01	2.9526E+01	2.9852E+01	2.9825E+01	2.9521E+01	2.9802E+01
	4	**3.5785E+01**	3.5602E+01	3.5362E+01	3.4259E+01	3.5521E+01	3.5652E+01	3.5452E+01	3.5632E+01	3.5521E+01
	5	**4.1256E+01**	4.1010E+01	4.1025E+01	4.1152E+01	4.1102E+01	4.1012E+01	4.1002E+01	4.1102E+01	4.1025E+01
35010	2	**2.8522E+01**	2.4521E+01	2.2365E+01	2.3029E+01	2.3326E+01	2.3026E+01	2.3159E+01	2.3025E+01	2.3013E+01
	3	**2.9956E+01**	2.1256E+01	2.8521E+01	2.9025E+01	2.9032E+01	2.9126E+01	2.9267E+01	2.9021E+01	2.9025E+01
	4	**3.5632E+01**	3.3256E+01	3.5021E+01	3.5020E+01	3.5125E+01	3.5362E+01	3.5021E+01	3.5110E+01	3.5032E+01
	5	4.0021E+01	4.0021E+01	4.0523E+01	4.0632E+01	**4.2550E+01**	4.0026E+01	4.0412E+01	4.0432E+01	4.0512E+01
113016	2	2.3652E+01	2.3232E+01	2.3762E+01	**2.4789E+01**	2.3562E+01	2.3326E+01	2.3705E+01	2.3702E+01	2.3706E+01
	3	3.0102E+01	3.0325E+01	**3.2562E+01**	3.0256E+01	3.0502E+01	3.0125E+01	3.0056E+01	3.0302E+01	3.0256E+01
	4	**3.8895E+01**	3.6258E+01	3.7023E+01	3.7056E+01	3.8002E+01	3.4256E+01	3.3621E+01	3.5422E+01	3.8362E+01
	5	**4.5895E+01**	4.4205E+01	4.2602E+01	4.3203E+01	4.4256E+01	4.2026E+01	4.3436E+01	4.2125E+01	4.4332E+01

Table 10 Iteration number of the optimal threshold at low threshold levels

Image	Thresholds	HVSFLA	ACOR	WOA	DE	BA	PSO	CGPSO	IGWO	LGCMFO
12003	2	**30**	35	88	92	83	56	49	89	46
	3	**25**	93	87	85	89	75	72	94	92
	4	**42**	59	56	89	69	94	85	88	82
	5	**36**	89	92	95	76	72	95	96	100
38082	2	**12**	35	36	42	81	38	29	77	49
	3	**18**	49	69	56	45	84	56	92	69
	4	65	92	91	**53**	85	86	65	92	62
	5	**43**	56	90	91	81	62	63	8	79
19021	2	58	41	92	**19**	62	90	48	89	34
	3	**25**	63	62	52	62	46	96	95	72
	4	**85**	95	93	95	89	94	86	96	100
	5	95	96	94	99	98	89	86	**84**	99
65010	2	**18**	5	48	46	74	29	48	92	66
	3	**24**	8	93	48	45	55	94	89	74
	4	**25**	94	93	48	85	77	75	93	65
	5	81	98	98	83	85	95	**71**	98	86
35010	2	**19**	69	48	86	74	76	34	72	44
	3	**25**	83	78	91	45	90	45	93	68
	4	**23**	93	92	56	67	68	64	93	68
	5	**25**	47	89	73	51	43	96	99	86
113016	2	**18**	49	64	28	59	83	56	79	39
	3	23	93	**17**	42	98	93	96	96	88
	4	90	96	68	98	**65**	89	97	98	96
	5	**40**	98	67	94	96	87	105	96	98

Table 11 The p-values of the HVSFLA compared to other algorithms at low threshold levels

Image	Thresholds	ACOR	WOA	DE	BA	PSO	CGPSO	IGWO	LGCMFO
12003	2	2.315E-02	4.738E-02	1.648E-02	4.052E-02	3.997E-02	4.523E-02	4.160E-02	2.299E-02
	3	4.403E-02	4.743E-02	2.125E-02	4.005E-02	4.003E-02	4.422E-02	4.926E-02	4.810E-02
	4	2.168E-02	3.716E-02	2.750E-02	2.165E-02	1.525E-02	3.195E-02	3.797E-02	3.701E-02

	5	3.282E-02	2.691E-02	2.435E-02	4.662E-02	5.107E-02	4.909E-02	4.668E-02	1.151E-02
38082	2	2.923E-02	4.162E-02	4.637E-02	4.816E-02	4.205E-02	1.742E-02	4.602E-02	4.482E-02
	3	3.693E-02	3.763E-02	1.257E-02	5.132E-02	2.773E-02	4.099E-02	3.420E-02	3.599E-02
	4	4.959E-02	4.788E-02	3.963E-02	3.867E-02	3.150E-02	2.303E-02	4.195E-02	1.295E-02
	5	4.776E-02	4.464E-02	1.814E-02	4.963E-02	3.861E-02	3.228E-02	4.438E-02	4.450E-02
19021	2	5.902E-02	2.783E-02	4.192E-02	2.645E-02	4.504E-02	4.220E-02	1.994E-02	2.651E-02
	3	2.174E-02	3.732E-02	1.838E-02	2.117E-02	4.712E-02	1.981E-02	2.977E-02	2.149E-02
	4	3.643E-02	2.733E-02	3.511E-02	2.562E-02	4.789E-02	2.519E-02	4.961E-02	1.570E-02
	5	1.257E-02	4.114E-02	4.997E-02	3.923E-02	2.946E-02	3.416E-02	3.012E-02	2.555E-02
65010	2	4.784E-02	4.983E-02	2.777E-02	4.150E-02	3.147E-02	2.689E-02	4.294E-02	2.142E-02
	3	4.010E-02	4.729E-02	1.235E-02	2.452E-02	5.782E-02	4.992E-02	4.507E-02	4.260E-02
	4	5.286E-02	1.628E-02	2.068E-02	3.013E-02	3.865E-02	4.937E-02	4.977E-02	1.331E-02
	5	5.941E-02	4.112E-02	2.989E-02	5.310E-02	4.249E-02	1.795E-02	4.266E-02	2.377E-02
35010	2	5.647E-02	1.126E-02	2.668E-02	4.074E-02	2.382E-02	2.184E-02	1.542E-02	2.409E-02
	3	3.048E-02	3.072E-02	2.148E-02	4.956E-02	4.112E-02	4.511E-02	1.181E-02	4.400E-02
	4	1.002E-02	4.657E-02	5.681E-02	2.018E-02	3.942E-02	2.877E-02	4.090E-02	3.222E-02
	5	3.704E-02	4.907E-02	4.416E-02	5.136E-02	4.817E-02	4.869E-02	3.836E-02	4.780E-02
113016	2	2.039E-02	2.836E-02	4.811E-02	4.379E-02	1.430E-02	4.862E-02	4.810E-02	4.016E-02
	3	2.096E-02	4.724E-02	3.190E-02	2.245E-02	3.502E-02	4.218E-02	4.731E-02	4.916E-02
	4	2.629E-02	4.461E-02	5.702E-02	3.379E-02	3.608E-02	4.300E-02	4.313E-02	1.570E-02
	5	1.480E-02	2.213E-02	1.029E-02	2.995E-02	1.451E-02	3.009E-02	3.617E-02	4.893E-02

HVSFLA：Segmented image and Jet colormap image

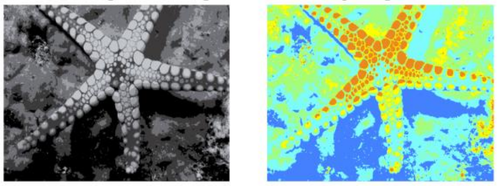

ACOR：Segmented image and Jet colormap image

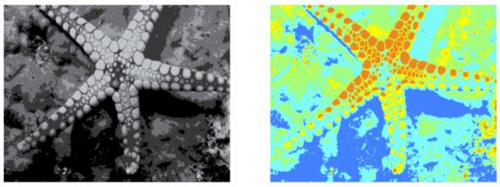

WOA：Segmented image and Jet colormap image

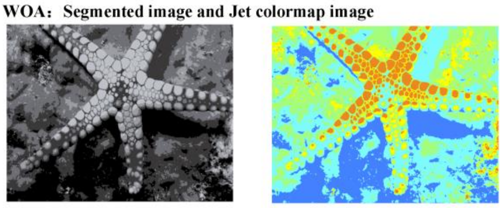

DE：Segmented image and Jet colormap image

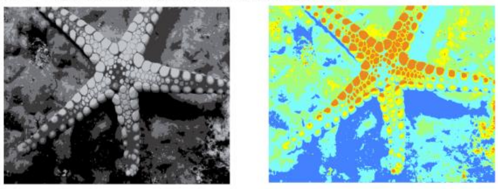

BA：Segmented image and Jet colormap image

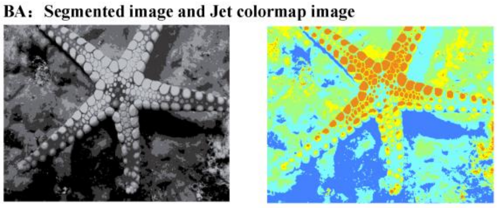

PSO：Segmented image and Jet colormap image

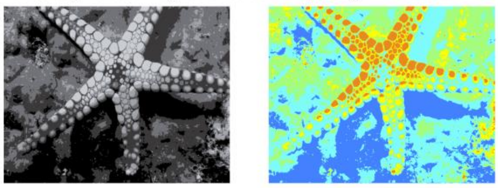

CGPSO：Segmented image and Jet colormap image

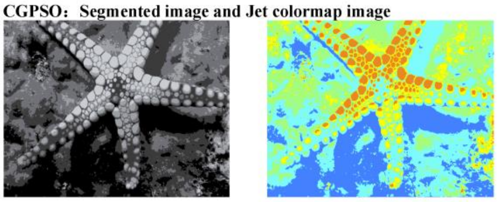

IGWO：Segmented image and Jet colormap image

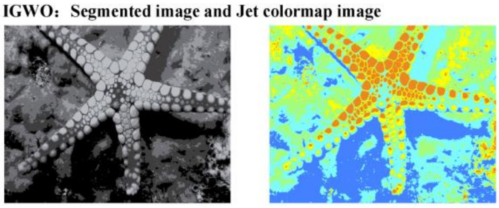

IGCMFO：Segmented image and Jet colormap image

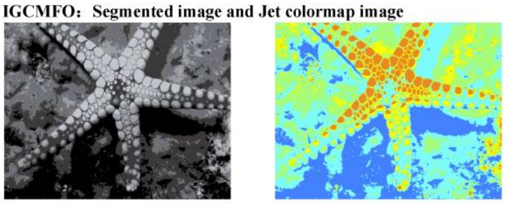

Figure 8. Segmented results of 12003 using all algorithms at threshold value 5

4.5.4 High-threshold experimental study

In this subsection, the proposed HVSFLA was performed at high threshold levels, 10, 15, 20, and 25, using images 12003, 38082, 19021, 65010, 35010, and 113016 to further analyze its performance. HVSFLA was compared with ACOR(Socha & Dorigo, 2008), WOA(Mirjalili & Lewis, 2016), DE(R. Storn & K. J. J. o. G. O. Price, 1997), BA(X.-S. Yang, 2010), PSO (Kennedy & Eberhart, 1995), CGPSO (Jia, et al., 2011), IGWO (Cai, et al., 2019), and LGCMFO (Xu, et al., 2019) . The AVG and STD of the results of PSNR, SSIM, and FSIM are listed in Table 12, 13, and 14, respectively, and the results of further analysis are shown in Table 15 and 16. At high threshold levels, the mean value of the overall ranking of HVSFLA still has the smallest values. According to the Wilcoxon signed-rank test, the proposed HVSFLA is still significantly superior to s other algorithms at high threshold levels.

Table 15 shows the maximum values of Kapur's entropy obtained by algorithms at high-level threshold segmentation, and Table 16 indicates the number of iterations to meet the optimum threshold. In terms of fitness, it can also be seen from Table 15 that the proposed HVSFLA has obvious advantages in finding a maximum entropy of Kapur relative to other successful algorithms while conducting high threshold segmentation experiments. As for the number of iterations, it can be seen from Table 16 that the proposed HVSFLA can also most efficiently reach the desired threshold, which also means that its convergence is the fastest at high threshold levels. Figure 9 presents the segmentation results of the proposed HVSFLA and other peers on the segmentation of the image 65010 at the threshold level 20. By analyzing and comparing detailed images in the segments, HVSFLA's original image information retention and segmentation effect performance are substantially better than other algorithms. In addition, the p-values of the HVSFLA compared to other algorithms at high threshold levels obtained by the Wilcoxon test are shown in Table 17, and it can be seen that most of the values are less than 0.05, indicating that the proposed HVSFLA is significantly different from other algorithms in terms of statistics at high threshold levels. The efficiency of the HVSFLA is verified based on the above results.

The proposed HVSFLA is significantly superior to other algorithms in terms of image detail retention and overall effect at high threshold levels. Moreover, it can perform faster than other algorithms to obtain the optimal threshold in finding Kapur's entropy. Therefore, it can be concluded that the HVSFLA has great potential for image segmentation at high threshold levels.

Table 12 The comparison results of PSNR at high threshold levels

Thresholds		HVSFLA	ACOR	WOA	DE	BA	PSO	CGPSO	IGWO	LGCMFO
10	+/−/=	~	3/0/3	2/0/4	3/0/3	3/1/2	3/2/1	3/2/1	5/0/1	4/1/1
	Mean	**1.6333**	3.0124	6.4532	5.0134	6.9632	5.2134	5.5987	8.1231	6.4212
	Rank	**1**	2	7	3	8	4	5	9	6
15	+/−/=	~	2/0/4	3/1/2	2/0/4	2/0/4	2/0/4	1/0/5	5/0/1	3/0/3
	Mean	**3.0543**	3.3321	7.3320	6.0124	6.8295	4.3321	4.1652	7.5921	6.1756
	Rank	**1**	2	8	5	7	4	3	9	6
20	+/−/=	~	4/0/2	5/0/1	2/0/4	5/0/1	2/0/4	2/0/4	5/0/1	3/0/3
	Mean	**3.1532**	3.6521	9.0325	4.6584	6.6532	4.0021	3.3421	8.8436	5.8452
	Rank	**1**	3	9	5	7	4	2	8	6
25	+/−/=	~	2/0/4	4/0/2	3/0/3	4/1/1	4/0/2	4/0/2	3/0/3	2/0/4
	Mean	**2.8321**	4.0125	8.3231	4.5652	7.6563	3.5215	3.5421	8.8321	5.1652
	Rank	**1**	4	8	5	7	2	3	9	6

Table 13 The comparison results of SSIM at high threshold levels

Thresholds		HVSFLA	ACOR	WOA	DE	BA	PSO	CGPSO	IGWO	LGCMFO
10	+/−/=	~	2/0/4	3/0/3	3/0/3	3/1/2	4/0/2	3/0/3	4/1/1	4/2/0
	Mean	**1.8321**	3.0230	6.5421	5.1562	7.0231	5.1125	5.6623	8.1562	6.5321
	Rank	**1**	2	7	4	8	3	5	9	6

15	+/−/=	~	3/0/3	3/1/2	2/0/4	2/0/4	4/0/1	5/1/0	5/0/1	3/2/1
	Mean	**3.1532**	3.3332	7.3231	6.0214	6.8231	4.3421	4.1562	7.6652	6.1632
	Rank	**1**	2	8	5	7	4	3	9	6
20	+/−/=	~	4/0/2	5/0/1	2/0/4	2/0/4	2/0/4	2/0/4	5/0/1	3/0/3
	Mean	**3.1521**	3.6625	9.0325	4.6652	6.6632	4.0425	3.3632	8.8352	5.8325
	Rank	**1**	3	9	5	7	4	2	8	6
25	+/−/=	~	5/0/1	4/0/2	3/0/3	4/0/2	4/0/2	4/0/2	3/0/3	2/0/4
	Mean	**2.8321**	4.0362	8.3325	4.5258	7.6635	3.5258	3.5235	8.8352	5.1652
	Rank	**1**	4	8	5	7	3	2	9	6

Table 14 The comparison results of FSIM at high threshold levels

Thresholds		HVSFLA	ACOR	WOA	DE	BA	PSO	CGPSO	IGWO	LGCMFO
10	+/−/=	~	2/0/4	3/0/3	3/0/3	3/1/2	5/0/1	3/0/3	5/1/2	4/0/2
	Mean	**1.8325**	3.0258	6.5026	5.1632	7.0369	5.1582	5.6652	8.1658	6.5002
	Rank	**1**	2	7	4	8	3	5	9	6
15	+/−/=	~	3/0/3	3/1/2	2/1/3	2/1/3	1/1/4	0/1/5	6/0/0	3/0/3
	Mean	**3.1652**	3.3325	7.3328	6.0258	6.8236	4.3589	4.1456	7.6582	6.1598
	Rank	**1**	2	8	5	7	4	3	9	6
20	+/−/=	~	4/0/2	5/0/1	2/0/4	1/0/5	1/1/4	2/3/1	5/0/1	3/0/3
	Mean	**3.1659**	3.6696	9.0365	4.6568	6.6756	4.0362	3.3125	8.8456	5.8456
	Rank	**1**	3	9	5	7	4	2	8	6
25	+/−/=	~	5/0/1	4/0/2	2/0/4	4/0/2	3/0/3	4/0/2	3/0/3	3/1/3
	Mean	**2.8362**	4.0325	8.3325	4.5456	7.6652	3.5325	3.5452	8.8452	5.1569
	Rank	**1**	4	8	5	7	2	3	9	6

Table 15 The fitness value results at high threshold levels

Image	Thresholds	HVSFLA	ACOR	WOA	DE	BA	PSO	CGPSO	IGWO	LGCMFO
12003	10	6.3569E+01	6.2746E+01	6.0026E+01	6.0258E+01	**6.8362E+01**	6.0125E+01	6.0325E+01	6.3029E+01	6.2452E+01
	15	7.9854E+01	**8.3698E+01**	7.7321E+01	7.6325E+01	7.5623E+01	7.6325E+01	7.4521E+01	7.90E+01	7.5121E+01
	20	**9.6521E+01**	9.2754E+01	9.0007E+01	9.0024E+01	8.9032E+01	8.8521E+01	9.0524E+01	9.3125E+01	8.4201E+01
	25	**1.2587E+02**	1.0126E+02	1.0021E+02	1.0256E+01	1.0021E+01	1.0001E+02	1.004E+02	1.0325E+02	9.6752E+01
38082	10	**7.7854E+01**	7.5623E+01	7.5632E+01	7.6598E+01	7.5785E+01	7.2956E+01	7.6325E+01	7.5231E+01	7.3658E+01
	15	**8.4526E+01**	8.0302E+01	8.0321E+01	8.0256E+01	8.2084E+01	8.2035E+01	8.2025E+01	8.0369E+01	7.8521E+01
	20	**9.8989E+01**	9.4587E+01	9.2351E+01	9.5388E+01	9.5236E+01	9.2541E+01	9.3854E+01	9.5623E+01	9.0625E+01
	25	1.0502E+02	1.0425E+02	1.0005E+02	1.0325E+02	1.0032E+02	1.0325E+02	1.0215E+02	**1.0929E+02**	1.0254E+01
19021	10	**5.9856E+01**	5.5698E+01	5.7123E+01	5.6529E+01	5.7541E+01	5.7854E+01	5.5413E+01	5.8025E+01	5.5521E+01
	15	**7.8547E+01**	7.4251E+01	7.4256E+01	7.2365E+01	7.5026E+01	7.4326E+01	7.3687E+01	7.362E+01	6.9269E+01
	20	**9.2659E+01**	8.7758E+01	8.8852E+01	8.7325E+01	8.8854E+01	8.6325E+01	8.6800E+01	8.7452E+01	8.0029E+01
	25	**1.2569E+02**	1.0056E+01	1.0102E+02	1.0001E+02	1.0126E+02	1.0548E+01	1.0027E+01	1.0032E+01	1.0367E+01
65010	10	6.3805E+01	**6.4956E+01**	6.3985E+01	6.3857E+01	6.3865E+01	6.3854E+01	6.3654E+01	6.3703E+01	6.229E+01
	15	**8.6587E+01**	8.1236E+01	8.1575E+01	8.1259E+01	8.2368E+01	8.2257E+01	8.2364E+01	8.1985E+01	7.8547E+01
	20	**9.8658E+01**	9.7562E+01	9.5641E+01	9.7125E+01	9.8514E+01	9.5874E+01	9.6125E+01	9.7856E+01	9.0324E+01
	25	1.1003E+02	1.0026E+02	**1.2059E+02**	1.0885E+02	1.1002E+02	1.08521E+02	1.0754E+02	1.0025E+02	1.0014E+02
35010	10	**6.5896E+01**	6.3254E+01	6.3254E+01	6.3569E+01	6.3752E+01	6.3564E+01	6.3521E+01	6.3754E+01	6.1254E+01
	15	**8.8547E+01**	8.3254E+01	8.2002E+01	8.2541E+01	8.3215E+01	8.2365E+01	8.2254E+01	8.2552E+01	7.8352E+01
	20	**9.9989E+01**	9.6554E+01	9.8352E+01	9.7325E+01	9.8687E+01	9.6698E+01	9.6654E+01	9.7805E+01	9.0895E+01
	25	**1.6542E+02**	1.0754E+02	1.1025E+02	1.0908E+02	1.1254E+02	1.0885E+02	1.0365E+02	1.0802E+02	1.0369E+02
113016	10	**6.9878E+01**	6.6584E+01	6.6685E+01	6.7458E+01	6.5847E+01	6.8254E+01	6.8956E+01	6.3654E+01	6.8541E+01
	15	**8.8854E+01**	8.6854E+01	8.4954E+01	8.5654E+01	8.6595E+01	8.6584E+01	8.5023E+01	8.5421E+01	8.2541E+01
	20	**1.2156E+02**	1.0135E+02	1.0325E+01	1.0785E+01	1.0064E+02	1.0547E+01	1.0052E+02	1.0251E+02	1.0652E+01
	25	**1.3698E+02**	1.1029E+02	1.1009E+02	1.1078E+02	1.1074E+02	1.0882E+02	1.1074E+02	1.1165E+02	1.2584E+02

Table 16 Iteration number of the optimal threshold at high threshold levels

Image	Thresholds	HVSFLA	ACOR	WOA	DE	BA	PSO	CGPSO	IGWO	LGCMFO
12003	10	**28**	35	84	97	86	64	45	96	45
	15	**21**	95	84	83	96	70	65	96	97
	20	88	55	**32**	97	64	93	84	95	83
	25	**65**	96	93	94	72	74	93	94	100
38082	10	**12**	38	45	29	83	45	37	76	56
	15	**18**	47	76	47	42	84	53	96	65

	20	76	95	93	**59**	92	79	68	93	74
	25	**29**	64	91	92	81	67	68	94	87
19021	10	56	44	92	**18**	68	92	54	82	46
	15	**28**	65	69	65	62	46	92	96	72
	20	**83**	90	90	92	88	97	84	93	93
	25	95	94	97	94	96	**89**	97	94	91
65010	10	**18**	42	45	42	64	28	41	90	67
	15	**24**	78	97	59	39	58	95	93	65
	20	**25**	92	95	35	81	73	72	94	65
	25	85	98	92	86	82	97	**73**	98	83
35010	10	**19**	68	46	88	75	66	29	79	57
	15	**26**	83	75	93	48	95	46	97	68
	20	**23**	94	96	58	69	68	63	91	69
	25	**26**	48	84	78	52	44	95	98	88
113016	10	**18**	36	62	29	49	86	46	85	38
	15	**23**	92	27	47	96	98	95	98	87
	20	89	96	69	98	**62**	89	87	98	87
	25	**40**	98	64	92	93	87	98	96	94

Table 17 The p-values of the HVSFLA compared to other algorithms at high threshold levels

Image	Thresholds	ACOR	WOA	DE	BA	PSO	CGPSO	IGWO	LGCMFO
12003	2	4.421E-02	2.243E-02	3.810E-02	1.227E-02	4.551E-02	2.802E-02	4.752E-02	1.036E-02
	3	2.531E-02	2.635E-02	2.609E-02	3.343E-02	4.372E-02	2.894E-02	1.559E-02	4.260E-02
	4	1.339E-02	3.832E-02	1.727E-02	1.697E-02	4.595E-02	4.799E-02	2.576E-02	1.562E-02
	5	3.935E-02	1.575E-02	4.425E-02	3.914E-02	4.756E-02	1.334E-02	4.922E-02	4.519E-02
38082	2	2.328E-02	4.485E-02	3.337E-02	3.137E-02	4.262E-02	2.119E-02	3.579E-02	1.382E-02
	3	4.359E-02	1.333E-02	2.494E-02	2.012E-02	1.005E-02	2.788E-02	4.586E-02	2.410E-02
	4	2.487E-02	2.847E-02	1.887E-02	4.668E-02	1.012E-02	3.350E-02	2.929E-02	3.374E-02
	5	4.313E-02	1.122E-02	1.876E-02	4.033E-02	1.350E-02	4.511E-02	1.056E-02	3.341E-02
19021	2	1.706E-02	4.013E-02	3.089E-02	4.548E-02	2.043E-02	2.876E-02	3.492E-02	3.671E-02
	3	1.518E-02	3.800E-02	2.734E-02	1.275E-02	1.091E-02	2.750E-02	1.924E-02	3.592E-02
	4	4.520E-02	1.858E-02	3.965E-02	1.734E-02	2.696E-02	3.985E-02	3.110E-02	2.733E-02
	5	1.176E-02	3.720E-02	1.282E-02	3.948E-02	2.364E-02	2.872E-02	3.900E-02	1.559E-02
65010	2	3.747E-02	3.229E-02	4.389E-02	3.787E-02	3.165E-02	4.443E-02	3.430E-02	4.008E-02
	3	3.935E-02	4.403E-02	3.720E-02	4.108E-02	4.705E-02	2.866E-02	3.353E-02	1.967E-02
	4	2.749E-02	3.234E-02	1.547E-02	3.008E-02	2.194E-02	2.992E-02	2.734E-02	3.602E-02
	5	2.519E-02	4.607E-02	4.434E-02	2.702E-02	2.352E-02	2.950E-02	1.977E-02	4.429E-02
35010	2	4.919E-02	2.678E-02	1.799E-02	3.445E-02	4.438E-02	1.918E-02	2.716E-02	1.337E-02
	3	2.596E-02	2.433E-02	3.429E-02	4.423E-02	2.362E-02	1.342E-02	1.041E-02	4.888E-02
	4	2.761E-02	2.956E-02	3.172E-02	3.683E-02	1.552E-02	1.270E-02	3.435E-02	1.126E-02
	5	1.627E-02	2.024E-02	1.649E-02	3.094E-02	3.031E-02	4.554E-02	4.832E-02	4.342E-02
113016	2	2.304E-02	4.717E-02	1.023E-02	2.195E-02	4.427E-02	1.933E-02	1.382E-02	4.343E-02
	3	2.256E-02	2.867E-02	4.086E-02	3.816E-02	2.537E-02	4.446E-02	1.142E-02	1.199E-02
	4	4.578E-02	2.016E-02	4.059E-02	2.526E-02	3.783E-02	3.847E-02	4.545E-02	3.184E-02
	5	1.988E-02	2.725E-02	2.684E-02	3.271E-02	3.512E-02	4.491E-02	1.988E-02	4.773E-02

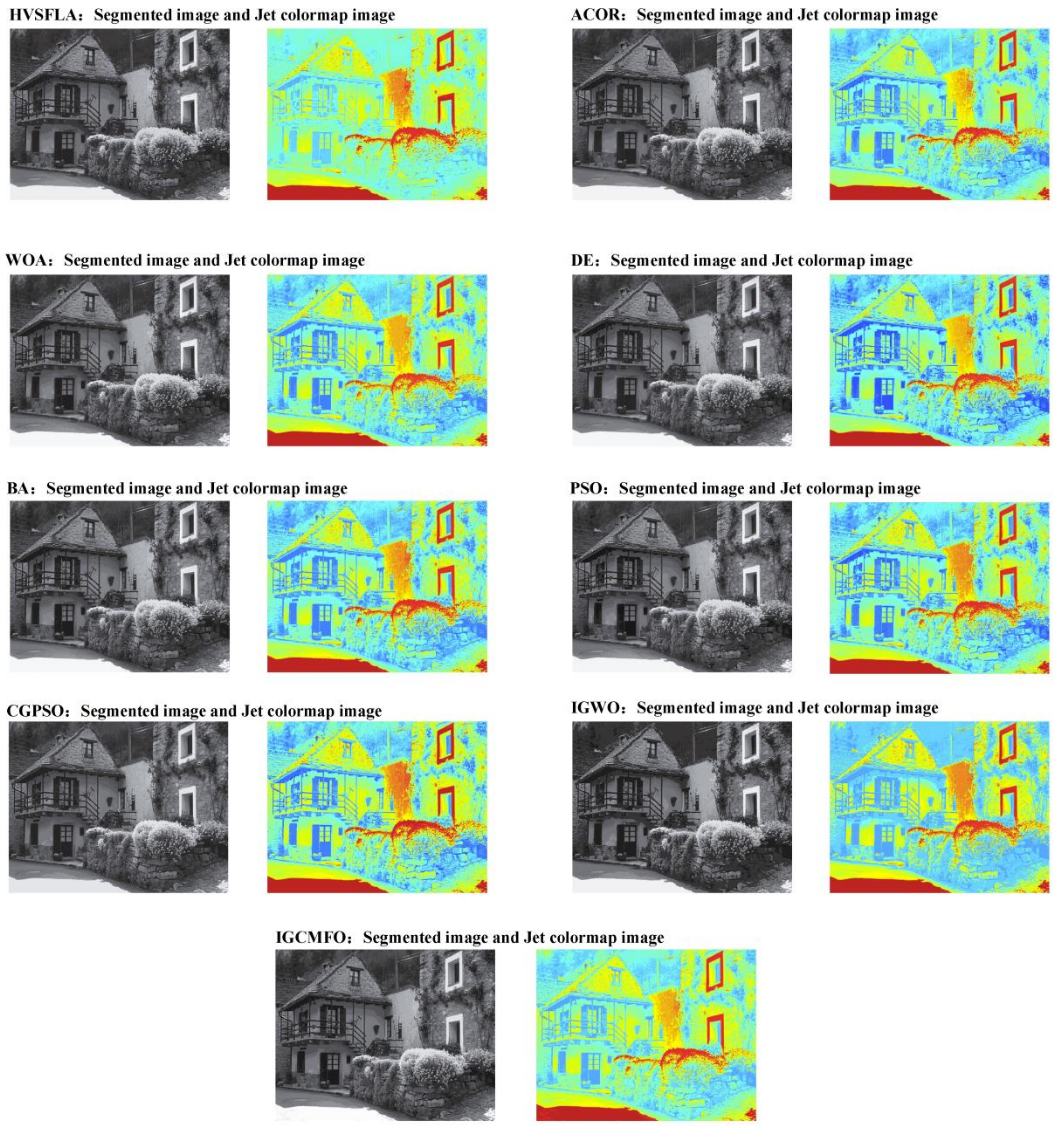

Figure 9. Segmented results of image 65010 using all algorithms at the threshold level 20.

5 Application to breast invasive ductal carcinoma image segmentation

According to the World Health Organization, breast cancer is one of the most commonly occurring malignant tumors in women. Therefore, it is crucial for the efficient diagnosis of this type of breast cancer. The pathological images of breast invasive ductal carcinoma play a critical role in diagnosing breast cancer patients and later radiotherapy and chemotherapy. Accordingly, for the successful use of the image to complete the auxiliary diagnosis and later treatment of the disease, how to do efficient segmentation analysis on the pathological image of breast invasive ductal carcinoma is of great importance and is also the most important step in completing the diagnostic use of the pathological image. In this section, the proposed HVSFLA was used to segment eight breast invasive ductal carcinoma pathological images from a histopathological image dataset (Bolhasani, Amjadi, Tabatabaeian, & Jassbi, 2020). In this experiment, the HVSFLA was compared with several other algorithms including ACOR, WOA, DE, BA, PSO, CGPSO, IGWO, and LGCMFO. The AVG and STD of the SSIM, FSIM and PSNR evaluation results obtained after 30 independent executions for various images obtained at different threshold levels by all methods are shown in Tables 16-18, respectively, where AVG and STD obtained by HVSFLA at different threshold levels are extremely well recorded. Among them, HVSFLA can obtain the best analysis results at low threshold levels and better handle the segmentation of breast invasive ductal carcinoma pathological images at t high-threshold levels. Table 19 shows the comprehensive evaluation results of SSIM, FSIM, and PSNR for all thresholds, and the proposed HVSFLA can all achieve better segmentation results than other algorithms in multiple perspectives. Table 20 shows the fitness entropy obtained by all the algorithms on breast invasive ductal carcinoma pathological images. The proposed HVSFLA shows obvious superiority over other algorithms at both low and high threshold levels. Figures 10-11 give detailed segmentation results at both the low threshold level 2 and the high threshold level 25; it can be seen that HVSFLA has a better segmentation ability for breast invasive ductal carcinoma pathological images, and it is an excellent segmentation method with high-quality results on this application. In addition, the p-values of the HVSFLA compared to other algorithms obtained by the Wilcoxon test on breast invasive ductal carcinoma image segmentation are shown in Table 21. It can be seen from this Table that most of the values are less than 0.05, indicating that HVSFLA significantly outperforms other algorithms on most of the test samples. These results demonstrate the efficiency of the proposed HVSFLA.

It can be concluded that the proposed algorithm HVSFLA has a tremendous potential capability for breast invasive ductal carcinoma image segmentation and may serve as assistive technology for breast invasive ductal carcinoma treatment in follow-up chemotherapy and radiotherapy.

Table 16 The PSNR comparison results

Thresholds		HVSFL	ACOR	WOA	DE	BA	PSO	CGPSO	IGWO	LGCMFO
2	+/−/	~	1/0/8	4/1/4	7/0/2	5/1/3	5/2/2	8/0/1	4/0/5	7/0/2
	Mean	**2.6021**	3.8023	4.3045	7.9032	4.6043	5.6042	8.5021	4.4054	6.5054
	Rank	**1**	2	3	8	5	6	9	4	7
3	+/−/	~	1/0/8	1/0/8	8/0/1	6/2/1	5/3/1	7/0/3	8/1/0	7/1/1
	Mean	**2.5032**	3.2123	3.5634	7.8056	5.2478	4.6845	5.8954	6.8953	6.8758
	Rank	**1**	2	3	9	5	4	6	8	7
4	+/−/	~	2/0/7	1/0/8	6/2/1	5/2/2	6/0/3	7/0/2	6/3/0	7/0/2
	Mean	**2.0021**	4.5245	3.2654	4.8967	4.6545	5.6367	7.5667	6.5367	8.5243
	Rank	**1**	3	2	5	4	6	8	7	9
5	+/−/	~	3/3/3	4/3/2	5/0/4	6/2/1	7/0/2	5/3/1	8/0/1	7/1/1
	Mean	**2.3235**	2.6543	4.2545	4.6956	4.8967	5.6367	4.3532	9.8534	6.8945
	Rank	**1**	2	3	5	6	7	4	9	8
10	+/−/	~	3/2/4	1/2/6	4/3/1	6/1/1	7/0/2	5/0/4	6/0/3	4/0/5
	Mean	**3.2545**	3.9845	3.6967	4.0278	6.9878	8.9554	4.6943	5.6954	4.3632
	Rank	**1**	3	2	4	8	9	6	7	5
15	+/−/	~	1/0/8	3/0/6	2/2/5	4/0/5	6/0/3	7/1/1	8/0/1	8/1/0
	Mean	**3.2521**	3.9835	4.3656	4.2565	6.3265	6.7554	8.3556	9.6543	8.5845
	Rank	**1**	2	4	3	5	6	7	9	8
20	+/−/	~	3/2/4	2/0/7	3/0/6	5/0/4	8/1/0	3/0/5	7/0/2	8/0/1
	Mean	**2.3602**	2.6953	2.6521	3.2154	3.2569	8.9562	3.5874	4.6985	5.6985
	Rank	**1**	3	2	4	5	9	6	7	8
25	+/−/	~	3/2/4	2/0/7	3/0/6	7/1/1	8/0/1	8/0/1	6/0/3	5/0/4
	Mean	**1.0221**	2.3680	2.3625	2.3698	4.6980	4.98521	8.9654	4.6251	3.6589
	Rank	**1**	3	2	4	7	8	9	6	5

Table 17 The SSIM comparison results

Thresholds		HVSFLA	ACOR	WOA	DE	BA	PSO	CGPSO	IGWO	LGCMFO
2	+/−/	~	1/0/8	1/0/8	6/0/3	7/1/1	6/2/1	7/0/2	4/0/5	7/2/0
	Mean	**2.03500**	3.5621	2.2154	6.5231	6.5897	4.2651	6.9856	3.6521	7.8521
	Rank	**1**	3	2	6	7	5	8	4	9
3	+/−/	**~**	2/0/7	2/2/5	6/0/3	7/1/1	6/2/1	8/0/1	5/0/4	8/1/0
	Mean	**1.5622**	2.3652	3.5987	5.3698	6.9854	6.3698	9.6587	5.3214	7.8562
	Rank	**1**	2	3	5	7	6	9	4	8
4	+/−/	**~**	1/0/8	6/1/2	6/0/3	7/2/0	3/1/5	7/0/2	8/0/1	6/0/3
	Mean	**2.1254**	3.5698	4.5214	5.6321	6.2541	3.6598	9.8590	9.9952	6.3254
	Rank	**1**	2	4	5	7	3	8	9	6

5	+/−/	~	3/0/6	2/0/7	6/0/3	6/1/2	7/2/0	8/0/1	9/0/0	8/0/1
	Mean	**2.1252**	3.2564	2.3541	5.6321	4.5623	6.3251	8.6359	9.8952	7.5214
	Rank	**1**	3	2	5	4	6	8	9	7
10	+/−/	~	1/1/7	2/0/7	6/0/3	5/0/4	6/1/2	7/0/2	7/1/1	8/0/1
	Mean	2.3121	**2.06521**	3.6521	5.6321	4.2598	6.3251	7.5214	8.6521	9.6587
	Rank	2	**1**	3	5	4	6	7	8	9
15	+/−/	~	1/2/6	2/1/6	6/0/3	5/2/2	5/1/3	8/1/0	6/0/3	7/1/1
	Mean	**1.0210**	2.3652	3.2514	5.6321	3.5621	4.5621	8.5621	6.5984	6.3251
	Rank	**1**	2	3	6	4	5	9	7	8
20	+/−/	~	2/0/7	1/1/7	3/0/6	8/0/1	7/1/1	8/1/0	6/0/3	7/0/2
	Mean	**2.3541**	3.6598	2.6541	5.3621	8.9951	6.9854	8.5632	5.6324	7.5621
	Rank	1	3	2	4	9	6	8	5	7
25	+/−/	~	1/1/7	2/1/6	7/1/1	6/0/3	8/0/1	9/0/0	8/0/1	7/0/2
	Mean	**1.2000**	2.3652	2.5412	4.3210	4.1254	6.3521	9.6584	7.85421	5.6321
	Rank	**1**	2	3	5	4	7	9	8	6

Table 18 The FSIM comparison results

Thresholds		HVSFLA	ACOR	WOA	DE	BA	PSO	CGPSO	IGWO	LGCMFO
2	+/−/	~	2/0/7	2/1/6	5/0/4	6/1/2	7/2/0	8/1/0	5/0/4	8/0/1
	Mean	**2.1521**	2.3210	2.2569	3.6521	4.5210	6.3521	8.5214	3.8541	9.5621
	Rank	**1**	3	2	4	6	7	8	5	9
3	+/−/	~	1/0/8	2/0/7	6/0/3	6/1/2	5/0/4	9/0/0	5/0/4	8/0/1
	Mean	**1.2100**	1.3210	3.2514	6.9854	6.3214	4.2563	8.5214	5.3698	7.3214
	Rank	**1**	2	3	7	6	4	9	5	8
4	+/−/	~	3/0/6	3/1/5	2/0/7	2/1/6	7/2/0	8/0/1	8/0/1	7/0/2
	Mean	**3.2514**	4.3254	4.2140	3.9854	3.6542	5.6321	7.0021	8.6254	6.9874
	Rank	**1**	5	4	3	2	6	8	9	7
5	+/−/	~	2/0/7	3/1/5	7/0/2	8/1/0	6/2/1	8/1/0	8/0/1	9/0/0
	Mean	**1.0201**	2.3695	3.2547	4.5214	5.3287	3.3321	6.5985	6.6621	7.8521
	Rank	**1**	2	3	5	6	4	7	8	9
10	+/−/	~	1/1/7	2/1/6	7/0/2	6/1/2	7/2/0	8/1/0	8/0/1	4/2/3
	Mean	**2.3621**	2.6548	3.6521	6.5214	4.5632	5.3254	7.5641	8.6541	3.8541
	Rank	**1**	2	3	7	5	6	8	9	4
15	+/−/	~	3/0/6	2/1/6	8/0/1	6/1/2	7/2/0	7/0/2	8/0/1	8/1/0
	Mean	**1.0000**	1.9854	1.3652	9.6521	2.3698	2.6854	3.6987	6.9874	4.5214
	Rank	**1**	3	2	9	4	5	6	8	7
20	+/−/	~	1/0/8	1/2/6	2/1/6	5/1/3	6/2/1	8/0/1	8/0/1	7/1/1
	Mean	**1.3621**	3.6548	2.3652	3.9854	4.5214	4.6321	8.6521	6.3541	6.5241
	Rank	**1**	3	2	4	5	6	9	8	7
25	+/−/	~	2/0/7	3/0/6	7/0/2	6/0/3	5/2/2	8/1/0	7/0/1	8/0/1
	Mean	**3.2541**	3.5632	3.9854	6.5231	4.89541	4.6321	7.8521	6.8541	8.5698
	Rank	**1**	2	3	6	5	4	8	7	9

Table 19 The average value of metric overall comparison result

Metric	HVSFLA	ACOR	WOA	DE	BA	PSO	CGPSO	IGWO	LGCMFO
PSNR	24.6	23.1	22.45	23.22	21.58	20.15	23.21	21.54	22.56
SSIM	0.89	0.84	0.82	0.85	0.81	0.85	0.87	0.85	0.84
FSIM	0.965	0.944	0.921	0.951	0.921	0.955	0.960	0.941	0.925

Table 20 The fitness value results obtained by all methods

Image	Thresholds	HVSFLA	ACOR	WOA	DE	BA	PSO	CGPSO	IGWO	LGCMFO
No1	2	**2.9018E+01**	2.9018E+01	2.9018E+01	2.9018E+01	2.9017E+01	2.9018E+01	2.9018E+01	2.9018E+01	2.9017E+01
	3	**4.3321E+01**	4.3210E+01	4.3321E+01	4.1652E+01	4.1524E+01	4.1759E+01	4.2159E+01	4.1852E+01	4.1375E+01
	4	**5.4362E+01**	5.2654E+01	5.2985E+01	5.3012E+01	5.2514E+01	5.2158E+01	5.3026E+01	5.1854E+01	5.1412E+01
	5	**7.9548E+01**	7.9546E+01	7.9521E+01	7.8524E+01	7.6528E+01	7.6398E+01	7.9510E+01	7.2584E+01	7.4220E+01
	10	**9.4562E+01**	9.0125E+01	9.0128E+01	8.0169E+01	9.0358E+01	8.6521E+01	9.1014E+01	8.4652E+01	8.5660E+01
	15	**1.1582E+02**	1.0125E+02	1.0198E+02	1.0125E+02	1.0001E+02	9.5210E+01	1.0215E+02	9.4425E+01	9.9295E+01
	20	**2.7986E+01**	2.7654E+01	2.7652E+01	2.7421E+01	2.7656E+01	2.7602E+01	2.7429E+01	2.7629E+01	2.7478E+01
	25	**4.2196E+01**	4.2196E+01	4.1159E+01	4.0920E+01	4.0952E+01	4.0742E+01	4.1070E+01	4.1049E+01	4.0812E+01
No2	2	**2.6985E+01**	2.6541E+01	2.5214E+01	2.5136E+01	2.5162E+01	2.5125E+01	2.3251E+01	2.5001E+01	2.5284E+01
	3	**3.9033E+01**	3.9033E+01	3.9033E+01	3.9033E+01	3.9033E+01	3.8521E+01	3.8156E+01	3.7954E+01	3.7632E+01
	4	**4.8563E+01**	4.6352E+01	4.6254E+01	4.6258E+01	4.5821E+01	4.8052E+01	4.5985E+01	4.5471E+01	4.8748E+01
	5	**8.7854E+01**	8.5324E+01	8.6548E+01	8.2104E+01	8.3652E+01	8.3001E+01	8.0365E+01	8.0547E+01	8.0695E+01
	10	**9.2584E+01**	8.8521E+01	8.8236E+01	8.8033E+01	8.8521E+01	8.8632E+01	9.0147E+01	8.5963E+01	8.6321E+01
	15	**1.1258E+02**	1.0125E+02	1.0100E+02	9.3256E+01	1.0102E+02	9.6987E+01	1.0100E+02	9.6321E+01	9.5218E+01
	20	**7.7542E+01**	7.5643E+01	7.6076E+01	7.5223E+01	7.4564E+01	7.5417E+01	7.5894E+01	7.2769E+01	7.3673E+01
	25	**9.1298E+01**	8.8761E+01	8.9267E+01	8.8178E+01	8.7987E+01	8.6569E+01	8.8768E+01	8.5049E+01	8.5812E+01
No3	2	**2.8562E+01**	2.3652E+01	2.4258E+01	2.6985E+01	2.5984E+01	2.6025E+01	2.6521E+01	2.6001E+01	2.6025E+01
	3	**3.9459E+01**	3.9459E+01	3.9459E+01	3.9210E+01	3.9260E+01	3.9119E+01	3.9203E+01	3.9103E+01	3.9001E+01
	4	**5.2563E+01**	5.0012E+01	5.0062E+01	4.9058E+01	4.9069E+01	4.9002E+01	4.9006E+01	4.90652E+01	4.9625E+01
	5	**7.8526E+01**	7.6532E+01	7.6321E+01	7.5421E+01	7.5721E+01	7.4758E+01	7.6532E+01	7.4025E+01	7.4012E+01
	10	**9.2016E+01**	9.0325E+01	9.0254E+01	8.8854E+01	8.9526E+01	8.9658E+01	8.9863E+01	8.6524E+01	8.6352E+01
	15	1.0365E+02	**1.0652E+02**	1.0228E+02	1.0102E+02	1.0025E+02	1.0120E+02	1.0139E+02	9.7460E+01	9.8685E+01
	20	**9.4584E+01**	9.2125E+01	9.2543E+01	9.0654E+01	9.1112E+01	8.9765E+01	9.2012E+01	8.1234E+01	8.8765E+01
	25	**1.0675E+02**	1.0432E+02	1.0321E+02	1.0102E+02	1.0259E+02	1.0129E+02	1.0269E+02	9.8584E+01	9.6695E+01
No4	2	2.9458E+01	**2.9458E+01**	2.9405E+01	2.9406E+01	2.9406E+01	2.9458E+01	2.8632E+01	2.9258E+01	2.9421E+01
	3	**4.4521E+01**	4.3021E+01	4.3031E+01	4.2623E+01	4.2352E+01	4.1632E+01	4.2956E+01	4.2105E+01	4.1752E+01
	4	5.4069E+01	**5.4125E+01**	5.3029E+01	5.3269E+01	5.2857E+01	5.0670E+01	5.3635E+01	5.2608E+01	5.1952E+01
	5	**7.8965E+01**	7.4321E+01	7.8521E+01	7.4872E+01	7.3230E+01	7.2965E+01	7.7932E+01	7.2105E+01	7.3369E+01
	10	**9.0895E+01**	8.7541E+01	9.0621E+01	8.6402E+01	8.5301E+01	8.4425E+01	8.8305E+01	8.3106E+01	8.4520E+01
	15	**9.9958E+01**	9.7528E+01	9.9750E+01	9.6365E+01	9.6854E+01	9.7852E+01	9.7384E+01	9.3103E+01	9.1008E+01
	20	9.1258E+01	8.9857E+01	**9.1345E+01**	8.9598E+01	8.7125E+01	8.6698E+01	8.9654E+01	8.4754E+01	8.7584E+01
	25	**1.2584E+02**	9.8745E+01	1.0126E+02	9.9168E+01	9.7685E+01	9.6058E+01	1.0158E+02	9.4969E+01	9.3658E+01

No5	2	2.5858E+01	2.5858E+01	**2.5858E+01**	2.5682E+01	2.5726E+01	2.5621E+01	2.5762E+01	2.5752E+01	2.5801E+01
	3	**3.9652E+01**	3.9124E+01	3.9102E+01	3.9026E+01	3.9058E+01	3.8452E+01	3.9081E+01	3.8950E+01	3.8862E+01
	4	**5.0925E+01**	5.0625E+01	5.0632E+01	5.0425E+01	5.0385E+01	4.8852E+01	5.0652E+01	4.9854E+01	4.9852E+01
	5	**7.8521E+01**	7.6852E+01	7.7085E+01	7.5652E+01	7.6332E+01	7.4738E+01	7.7080E+01	7.3352E+01	7.4152E+01
	10	9.0125E+01	**9.2635E+01**	9.0352E+01	8.5896E+01	8.9632E+01	8.6462E+01	8.9898E+01	8.5520E+01	8.5236E+01
	15	1.0385E+02	**1.0485E+02**	1.0254E+02	1.0036E+02	9.9856E+01	9.9362E+01	1.0225E+02	9.5632E+01	9.4452E+01
	20	**5.4598E+01**	5.3425E+01	5.3308E+01	5.3258E+01	5.2854E+01	5.2065E+01	5.3025E+01	5.2521E+01	5.2102E+01
	25	**7.9865E+01**	7.9025E+01	7.9254E+01	7.8254E+01	7.8143E+01	7.6258E+01	7.9658E+01	7.6485E+01	7.5562E+01
No6	2	**2.6991E+01**	2.6991E+01	2.6991E+01	2.6991E+01	2.6991E+01	2.5962E+01	2.5936E+01	2.5987E+01	2.5986E+01
	3	**3.8956E+01**	3.8754E+01	3.8762E+01	3.8029E+01	3.8652E+01	3.8062E+01	3.8758E+01	3.8036E+01	3.8589E+01
	4	5.3652E+01	4.9854E+01	**5.4854E+01**	4.9856E+01	4.9458E+01	4.9698E+01	4.9852E+01	4.9056E+01	4.9263E+01
	5	**7.6852E+01**	7.5623E+01	7.6062E+01	7.5325E+01	7.4962E+01	7.5562E+01	7.5856E+01	7.2695E+01	7.3688E+01
	10	**9.0562E+01**	8.9856E+01	8.9520E+01	8.8126E+01	8.7854E+01	8.6477E+01	8.8765E+01	8.5369E+01	8.5952E+01
	15	**1.0321E+02**	1.0200E+02	1.0015E+02	9.8652E+01	9.8523E+01	9.6521E+01	1.0036E+02	9.4036E+01	9.4048E+01
	20	**4.1192E+01**	4.1192E+01	4.1189E+01	4.0919E+01	4.0989E+01	4.0737E+01	4.1069E+01	4.1048E+01	4.0812E+01
	25	**5.2386E+01**	5.2156E+01	5.2652E+01	5.1587E+01	5.1521E+01	5.0654E+01	5.2125E+01	5.0548E+01	5.0254E+01
No7	2	**2.8521E+01**	2.6002E+01	2.6002E+01	2.6002E+01	2.6002E+01	2.6045E+01	2.6036E+01	2.6032E+01	2.6031E+01
	3	**3.9586E+01**	3.9586E+01	3.9480E+01	3.9420E+01	3.9482E+01	3.9436E+01	3.9421E+01	3.9200E+01	3.9136E+01
	4	5.1365E+01	**5.3652E+01**	5.0852E+01	5.0652E+01	5.0532E+01	5.0525E+01	5.0780E+01	4.9602E+01	5.0063E+01
	5	**7.9956E+01**	7.8425E+01	7.8325E+01	7.7412E+01	7.6841E+01	7.4736E+01	7.8563E+01	7.5805E+01	7.5834E+01
	10	**9.5214E+01**	9.3652E+01	9.3362E+01	9.0852E+01	9.1025E+01	8.9532E+01	9.632E+01	8.7502E+01	8.8862E+01
	15	**1.0652E+02**	1.0025E+02	1.0254E+02	1.0321E+02	1.0202E+02	1.0125E+02	1.0236E+02	9.8445E+01	9.6713E+01
	20	**9.4096E+01**	9.1025E+01	9.3023E+01	9.1035E+01	9.1025E+01	8.9635E+01	9.1852E+01	9.0254E+01	8.6632E+01
	25	**1.0598E+02**	1.0231E+02	1.0021E+02	1.0036E+02	1.0254E+02	9.9254E+01	1.0465E+02	9.8562E+01	9.7065E+01
No8	2	**2.9518E+01**	2.9518E+01	2.9518E+01	2.9518E+01	2.9518E+01	2.9513E+01	2.9518E+01	2.9518E+01	2.9515E+01
	3	**4.2568E+01**	4.2568E+01	4.2365E+01	4.2245E+01	4.2263E+01	4.1652E+01	4.2362E+01	4.2152E+01	4.1852E+01
	4	**5.3852E+01**	5.3803E+01	5.3269E+01	5.3065E+01	5.3621E+01	5.23621E+01	5.3025E+01	5.2582E+01	5.2652E+01
	5	**7.9785E+01**	7.9985E+01	7.9254E+01	7.8362E+01	7.8258E+01	7.6158E+01	7.9652E+01	7.6462E+01	7.5821E+01
	10	9.4202E+01	**9.5231E+01**	9.3125E+01	9.1456E+01	9.1052E+01	8.9732E+01	9.1760E+01	9.0185E+01	8.6732E+01
	15	**1.0652E+02**	1.0203E+02	1.0301E+02	1.0032E+02	1.0101E+02	9.9032E+01	1.0329E+02	9.7354E+01	9.7021E+01
	20	**9.0365E+01**	8.9214E+01	8.9074E+01	8.8437E+01	8.8362E+01	8.7452E+01	8.9752E+01	8.5026E+01	8.5623E+01
	25	1.0215E+02	**1.0365E+02**	1.0121E+02	9.9220E+01	1.0032E+02	9.9021E+01	1.0002E+02	9.4651E+01	9.4454E+01

Table 21 The p-values of the HVSFLA compared to other algorithms

Image	Thresholds	ACOR	WOA	DE	BA	PSO	CGPSO	IGWO	LGCMFO
No1	2	1.085E-02	2.101E-02	3.006E-02	4.245E-02	1.634E-02	2.220E-02	1.651E-02	1.934E-02
	3	4.376E-02	1.024E-02	2.108E-02	3.307E-02	2.445E-02	4.159E-02	4.187E-02	1.385E-02
	4	2.152E-02	4.208E-02	3.136E-02	4.776E-02	3.967E-02	1.946E-02	1.455E-02	2.538E-02
	5	2.001E-02	2.990E-02	3.297E-02	4.486E-02	3.824E-02	1.937E-02	1.635E-02	3.001E-02
	10	2.954E-02	3.151E-02	2.651E-02	3.030E-02	3.804E-02	2.859E-02	2.423E-02	3.281E-02
	15	3.916E-02	4.484E-02	1.059E-02	4.155E-02	1.025E-02	3.478E-02	4.391E-02	4.907E-02
	20	1.810E-02	3.891E-02	3.811E-02	2.892E-02	2.497E-02	3.461E-02	3.331E-02	2.971E-02
	25	1.865E-02	3.672E-02	3.027E-02	4.315E-02	4.606E-02	1.490E-02	3.345E-02	2.604E-02
No2	2	4.905E-02	1.715E-02	2.525E-02	2.290E-02	2.273E-02	1.495E-02	4.703E-02	4.980E-02
	3	3.373E-02	3.202E-02	1.260E-02	4.905E-02	3.388E-02	2.138E-02	3.300E-02	2.044E-02
	4	2.218E-02	4.840E-02	2.434E-02	2.113E-02	2.191E-02	3.943E-02	1.040E-02	3.661E-02
	5	4.871E-02	3.384E-02	1.937E-02	1.291E-02	1.500E-02	2.645E-02	4.238E-02	4.857E-02
	10	4.584E-02	4.234E-02	1.814E-02	4.005E-02	2.553E-02	4.316E-02	3.435E-02	3.685E-02
	15	1.760E-02	4.938E-02	4.255E-02	4.325E-02	4.271E-02	4.740E-02	2.920E-02	2.197E-02
	20	1.007E-02	4.544E-02	2.574E-02	4.689E-02	4.925E-02	2.596E-02	2.074E-02	3.125E-02
	25	3.847E-02	1.855E-02	1.214E-02	2.308E-02	4.448E-02	1.209E-02	2.032E-02	1.006E-02
No3	2	4.471E-02	1.139E-02	2.500E-02	4.216E-02	1.335E-02	3.285E-02	2.924E-02	4.535E-02
	3	1.473E-02	2.804E-02	4.100E-02	3.153E-02	2.351E-02	3.991E-02	1.909E-02	2.618E-02
	4	1.156E-02	1.055E-02	1.661E-02	2.853E-02	1.945E-02	2.281E-02	1.194E-02	2.205E-02
	5	3.393E-02	2.895E-02	4.649E-02	4.283E-02	2.271E-02	2.972E-02	1.677E-02	4.802E-02
	10	3.417E-02	4.805E-02	2.277E-02	4.808E-02	4.938E-02	1.887E-02	2.034E-02	2.843E-02
	15	3.066E-02	1.996E-02	2.319E-02	1.305E-02	3.193E-02	4.757E-02	1.792E-02	2.151E-02
	20	1.030E-02	2.546E-02	1.817E-02	3.835E-02	3.997E-02	2.929E-02	3.423E-02	1.339E-02
	25	3.756E-02	2.726E-02	4.069E-02	1.940E-02	4.367E-02	3.160E-02	4.295E-02	3.329E-02
No4	2	4.784E-02	4.324E-02	1.280E-02	2.596E-02	1.668E-02	1.884E-02	4.242E-02	1.612E-02
	3	4.494E-02	4.299E-02	4.800E-02	2.072E-02	4.612E-02	1.384E-02	4.209E-02	1.292E-02
	4	1.453E-02	2.812E-02	1.633E-02	4.330E-02	1.420E-02	1.241E-02	3.832E-02	3.322E-02
	5	2.418E-02	2.522E-02	2.146E-02	4.981E-02	3.980E-02	4.278E-02	4.438E-02	2.148E-02
	10	1.968E-02	4.703E-02	3.749E-02	3.599E-02	3.917E-02	4.086E-02	4.124E-02	2.448E-02
	15	3.241E-02	3.963E-02	1.565E-02	3.816E-02	3.870E-02	1.783E-02	1.815E-02	3.899E-02
	20	3.451E-02	3.951E-02	3.048E-02	4.729E-02	1.534E-02	4.580E-02	4.973E-02	4.433E-02
	25	2.203E-02	4.788E-02	3.885E-02	3.751E-02	2.783E-02	3.737E-02	1.374E-02	2.392E-02

No5	2	4.193E-02	3.040E-02	4.715E-02	3.273E-02	3.035E-02	3.627E-02	3.602E-02	4.847E-02
	3	4.183E-02	4.168E-02	3.928E-02	2.523E-02	3.122E-02	4.962E-02	1.861E-02	4.814E-02
	4	4.124E-02	2.809E-02	3.999E-02	3.538E-02	4.439E-02	1.135E-02	1.975E-02	1.824E-02
	5	2.404E-02	4.397E-02	2.629E-02	2.453E-02	3.711E-02	2.697E-02	2.359E-02	4.073E-02
	10	1.217E-02	2.562E-02	1.958E-02	2.630E-02	4.223E-02	2.960E-02	1.791E-02	3.462E-02
	15	3.835E-02	3.954E-02	3.083E-02	2.475E-02	3.125E-02	3.334E-02	3.027E-02	4.676E-02
	20	4.972E-02	4.906E-02	1.876E-02	2.874E-02	4.824E-02	1.333E-02	4.803E-02	3.410E-02
	25	1.650E-02	3.093E-02	4.370E-02	3.014E-02	1.267E-02	3.641E-02	2.578E-02	3.809E-02
No6	2	1.454E-02	2.720E-02	3.652E-02	4.642E-02	3.166E-02	1.209E-02	3.338E-02	3.975E-02
	3	4.652E-02	1.829E-02	4.265E-02	1.826E-02	2.127E-02	3.227E-02	3.426E-02	2.540E-02
	4	2.927E-02	2.294E-02	4.176E-02	2.354E-02	2.924E-02	3.848E-02	3.859E-02	2.006E-02
	5	4.407E-02	1.443E-02	2.876E-02	3.297E-02	3.739E-02	2.952E-02	2.606E-02	1.147E-02
	10	4.240E-02	2.501E-02	2.238E-02	2.948E-02	1.833E-02	3.470E-02	4.435E-02	2.888E-02
	15	1.747E-02	2.320E-02	3.750E-02	2.049E-02	3.433E-02	1.855E-02	4.682E-02	3.580E-02
	20	1.989E-02	2.368E-02	4.947E-02	3.318E-02	2.305E-02	3.583E-02	4.003E-02	2.116E-02
	25	1.217E-02	4.268E-02	4.080E-02	4.513E-02	4.523E-02	2.523E-02	2.142E-02	3.071E-02
No7	2	3.436E-02	3.127E-02	4.318E-02	1.244E-02	1.534E-02	1.415E-02	4.187E-02	1.983E-02
	3	4.109E-02	3.084E-02	3.824E-02	2.764E-02	1.410E-02	2.510E-02	1.571E-02	2.190E-02
	4	3.044E-02	4.097E-02	3.381E-02	1.337E-02	4.836E-02	2.051E-02	3.018E-02	3.602E-02
	5	1.111E-02	1.481E-02	4.011E-02	3.253E-02	1.612E-02	1.965E-02	3.443E-02	4.566E-02
	10	4.962E-02	3.502E-02	2.987E-02	3.157E-02	1.610E-02	3.492E-02	3.815E-02	4.444E-02
	15	3.004E-02	2.387E-02	4.461E-02	4.072E-02	1.622E-02	3.092E-02	2.533E-02	1.840E-02
	20	2.328E-02	2.338E-02	1.272E-02	1.932E-02	1.358E-02	2.653E-02	3.915E-02	2.596E-02
	25	1.696E-02	3.298E-02	4.874E-02	3.349E-02	2.818E-02	1.871E-02	4.549E-02	4.552E-02
No8	2	3.503E-02	4.456E-02	1.395E-02	2.836E-02	3.676E-02	4.434E-02	1.223E-02	2.026E-02
	3	3.301E-02	1.794E-02	3.188E-02	4.444E-02	4.325E-02	4.444E-02	1.553E-02	4.867E-02
	4	4.004E-02	3.690E-02	2.612E-02	3.643E-02	4.161E-02	2.136E-02	4.452E-02	3.477E-02
	5	1.614E-02	4.607E-02	1.428E-02	2.416E-02	3.851E-02	3.462E-02	2.687E-02	1.661E-02
	10	2.427E-02	1.797E-02	3.897E-02	2.389E-02	2.890E-02	4.118E-02	2.645E-02	4.305E-02
	15	1.576E-02	2.193E-02	3.455E-02	2.015E-02	3.834E-02	4.819E-02	4.837E-02	3.623E-02
	20	4.402E-02	2.986E-02	4.132E-02	4.810E-02	4.832E-02	4.678E-02	4.001E-02	3.186E-02
	25	2.351E-02	4.560E-02	3.266E-02	2.193E-02	3.023E-02	2.539E-02	4.924E-02	2.005E-02

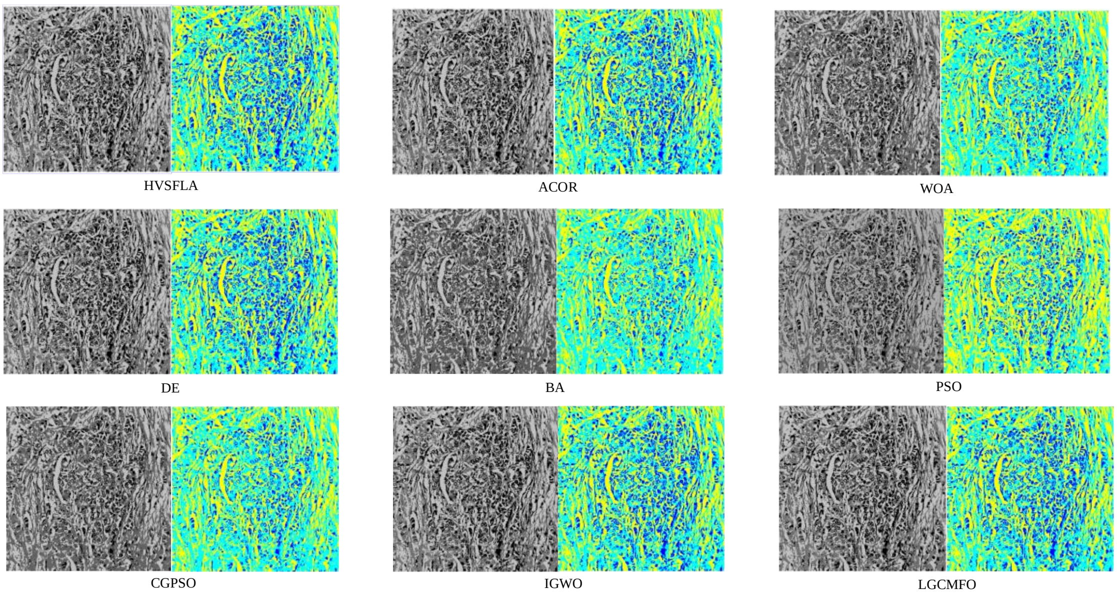

Fig 10. The segmented results of image obtained by all methods at low threshold level 2

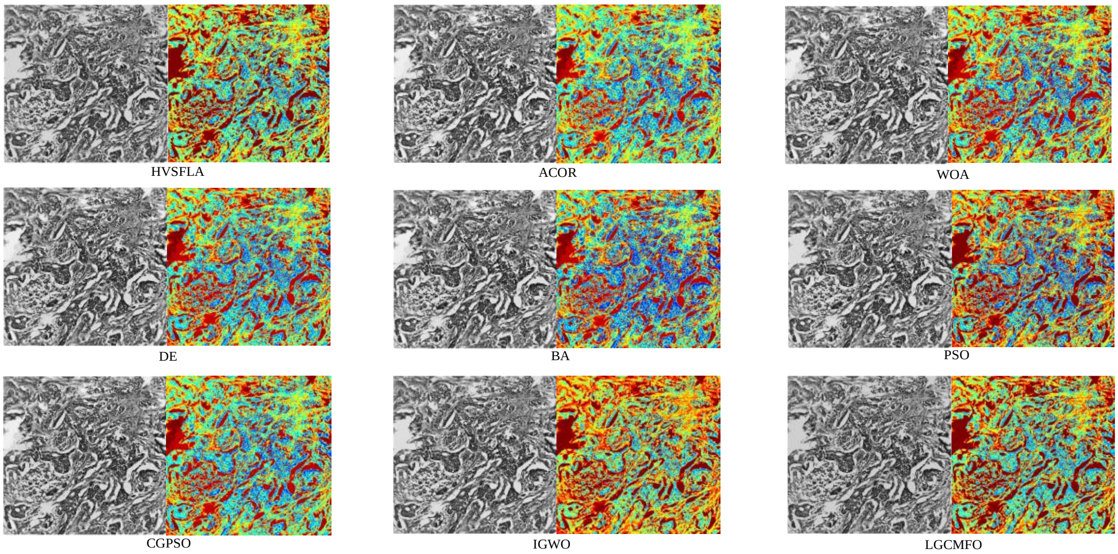

Fig 11. The segmented results of the image obtained by all methods at a high threshold level of 15

6 Discussion

In the component effect experiments the average ranking of all these strategy collocations on these CEC 2017 benchmark functions shows the HVSFLA can achieve the lowest ranking value of 1.46 and is ranked first, which implies the combination of horizontal and vertical crossover search outperforms single operator (horizontal or vertical crossover); Moreover, the diversity and the balance between the diversification and intensification capabilities of the HVSFLA and the original SFLA were investigated on these test functions, and both the diversification and intensification capabilities of HVSFLA are significantly improved compared with the basic SFLA, as shown in Figure 4 and Figure 5.

Furthermore, according to the results presented in Table 5, the proposed HVSFLA is significantly superior to the original SFLA and other competitors on most of the test functions. The theoretical optimal values on F1, F2, F3, F6, and F9 were all obtained by HVSFLA, besides the CLPSO, EPSDE, SaDE, and DE all acquire the theoretical optimal solution on F6 case. HVSFLA showed better performance than EPSDE on twenty-three functions, it performed similarly with EPSDE on two functions and was inferior to EPSDE on five test functions. HVSFLA performed better than SaDE on twenty-two functions, was inferior to SaDE on six test functions, and performed similarly with SaDE on two functions; HVSFLA was superior to GWO on twenty-nine functions and was inferior to GWO on only one function. HVSFLA had better performance than DE on twenty-nine functions. It shows a tie with DE on only one function. Notably, HVSFLA obtained the best convergence capability among all these algorithms. Horizontal crossover can encourage multiple frogs to share information, explore each frog and speed up the convergence rate efficiently. Meanwhile, vertical crossover search can aggressively make frogs in stagnation continue to search. Finally, a better balance can be ensured between diversification and intensification.

According to the results of the Berkeley segmentation dataset at low threshold levels and high threshold levels, by analyzing PSNR, SSIM, and FSIM, it can be seen that when HVSFLA is applied to the image segmentation field, segmentation at both low threshold levels and the high threshold levels, HVSFLA can achieve better threshold values and better stability in the segmentation process. According to the Wilcoxon signed-rank test, as shown in Tables 6-8 and Tables 11-13, the proposed HVSFLA is also significantly superior to other algorithms at both low threshold levels and high threshold levels. Regarding the application to breast invasive ductal carcinoma image segmentation in section 5, it can also be seen that the proposed HVSFLA still shows good performance at both low threshold levels and high threshold levels. However, the HVSFLA has some limitations. For example, the computational cost of the HVSFLA is increased. Due to the introduction of multiple strategies into HVSFLA, its computational time cost is slightly higher relative to the original SFLA. Therefore, parallel processing technologies can be considered to reduce its time complexity.

Another thing to consider is that no one algorithm can completely solve all practical problems as the no free lunch claims. However, the proposed HVSFLA performed well on benchmark functions and practical breast invasive ductal carcinoma images cases. Additional mechanisms may be needed to improve the HVSFLA further in order to apply it in more scenarios. Owing to its strong optimization ability, the proposed HVSFLA can also be applied to other optimization problems, including medical diagnosis (Hu, et al., 2021; Saber, Sakr, Abo-Seida, Keshk, & Chen, 2021), service ecosystem (Xue, et al., 2020), engineering optimization problems (X. Liang, et al., 2020), energy storage planning and scheduling (Cao, Cao, Gao, & Guan, 2021), active surveillance (Pei, Yang, Liu, & Chang, 2020), covert communication system (L. Zhang, et al., 2021), location-based services (Zongda Wu, Li, et al., 2021; Zongda Wu, Wang, Li, Lian, & Xu, 2020), information retrieval services (Zongda Wu, Renchao Li, et al., 2020; Zongda Wu, Shen, Lian, Su, & Chen, 2020; Zongda Wu, Shen, et al., 2021), kayak cycle phase segmentation (Qiu, Hao, et al., 2021), human motion capture (Qiu, Zhao, et al., 2021), image dehazing (X. Zhang, Wang, Wang, Tang, & Zhao, 2020), video deblurring (X. Zhang, Jiang, Wang, & Wang, 2021), tensor recovery (X. Zhang, Wang, Zhou, & Ma, 2019) and feature selection and learning (X. Zhang, Fan, Wang, Zhou, & Tao, 2021; Xiaoqin Zhang, et al., 2021).

7 Conclusions and future directions

In this research, the capability of SFLA to solve multi-threshold image segmentation problems was improved by implementing the horizontal and vertical crossover search mechanisms. In order to estimate its efficiency in solving these complex segmentation cases, the proposed HVSFLA was compared with several common algorithms on IEEE CEC 2017 benchmark functions. In addition, the capability of the proposed HVSFLA to solve multi-threshold image segmentation problems was thoroughly investigated at both low threshold levels (2, 3, 4, and 5) and high threshold levels (10, 15, 20, and 25) on six Berkeley segmentation images, and strict comparison experiments were also conducted with others algorithms. Finally, the proposed HVSFLA was applied to the segmentation of breast invasive ductal carcinoma images. In terms of solution efficiency and time complexity, the statistics showed that the established HVSFLA outperformed all competitors. Therefore, HVSFLA can be regarded as a promising method for multi-threshold segmentation of images, especially images of breast invasive ductal carcinoma.

In future work, our research plans to focus on the following points: for one thing, more strategies can be adopted to improve HVSFLA further, although the algorithm obtained reliable results on the CEC 2017 benchmark functions and successfully and efficiently solved one medical image segmentation cases in this study. For another, more medical image segmentation cases may be conducted by the proposed HVSFLA, and attempts can be made to extend it to more complicated optimization scenarios such as feature selection, multi-objective problems, and social manufacturing optimization.

Acknowledgments

This research was supported by the Key Project of Zhejiang Provincial Natural Science Foundation (LD21F020001, LZ22F020005) and the National Natural Science Foundation of China (U19A2061, U1809209, 62076185), Key Laboratory of Intelligent Image Processing and Analysis, Wenzhou, China (2021HZSY0071), and Taif University Researchers Supporting Project Number (TURSP-2020/125), Taif University, Taif, Saudi Arabia. We acknowledge the comments of the editor and anonymous reviewers that enhanced this manuscript significantly.

References

Abutaleb, A. S. (1989). Automatic thresholding of gray-level pictures using two-dimensional entropy. *Computer Vision, Graphics, and Image Processing, 47*, 22-32.

Ahmadianfar, I., Asghar Heidari, A., Gandomi, A. H., Chu, X., & Chen, H. (2021). RUN Beyond the Metaphor: An Efficient Optimization Algorithm Based on Runge Kutta Method. *Expert Systems with Applications*, 115079.

Bolhasani, H., Amjadi, E., Tabatabaeian, M., & Jassbi, S. J. (2020). A histopathological image dataset for grading breast invasive ductal carcinomas. *Informatics in Medicine Unlocked, 19*.

Buades, A., Coll, B., & Morel, J. (2005). A non-local algorithm for image denoising. In *2005 IEEE Computer Society Conference on Computer Vision and Pattern Recognition (CVPR'05)* (Vol. 2, pp. 60-65 vol. 62).

Cai, Z., Gu, J., Luo, J., Zhang, Q., Chen, H., Pan, Z., Li, Y., & Li, C. (2019). Evolving an optimal kernel extreme learning machine by using an enhanced grey wolf optimization strategy. *Expert Systems with Applications, 138*, 112814.

Cao, X., Cao, T., Gao, F., & Guan, X. (2021). Risk-Averse Storage Planning for Improving RES Hosting Capacity under Uncertain Siting Choice. *IEEE Transactions on Sustainable Energy*, DOI: 10.1109/TSTE.2021.3075615.

Chen, M., Zeng, G., Lu, K., & Weng, J. (2019). A Two-Layer Nonlinear Combination Method for Short-Term Wind Speed Prediction Based on ELM, ENN, and LSTM. *Ieee Internet of Things Journal, 6*, 6997-7010.

Chen, W., Zhang, J., Lin, Y., Chen, N., Zhan, Z., Chung, H. S., Li, Y., & Shi, Y. (2013). Particle Swarm Optimization With an Aging Leader and Challengers. *IEEE Transactions on Evolutionary Computation, 17*, 241-258.

Eusuff, M. M., & Lansey, K. E. (2003). Lansey, K.: Optimization of Water Distribution Network Design Using the Shuffled Frog Leaping Algorithm. Journal of Water Resources Planning and Management 129(3), 10-25. *Journal of Water Resources Planning & Management, 129*.

Fan, C., Ouyang, H., Zhang, Y., & Xiao, L. (2014). Optimal multilevel thresholding using molecular kinetic theory optimization algorithm. *Applied Mathematics and Computation, 239*, 391-408.

Fan, Y., Wang, P., Heidari, A. A., Zhao, X., Turabieh, H., & Chen, H. (2021). Delayed dynamic step shuffling frog-leaping algorithm for optimal design of photovoltaic models. *Energy Reports, 7*, 228-246.

Feng, S., Zuo, C., Zhang, L., Yin, W., & Chen, Q. (2021). Generalized framework for non-sinusoidal fringe analysis using deep learning. *Photonics Research, 9*, 1084-1098.

Feng, Y., Zhao, H., Li, X., Zhang, X., & Li, H. (2017). A multi-scale 3D Otsu thresholding algorithm for medical image segmentation. *Digital Signal Processing: A Review Journal, 60*, 186-199.

Heidari, A. A., Mirjalili, S., Faris, H., Aljarah, I., Mafarja, M., & Chen, H. (2019). Harris hawks optimization: Algorithm and applications. *Future Generation Computer Systems-the International Journal of Escience, 97*, 849-872.

Hu, Z., Wang, J., Zhang, C., Luo, Z., Luo, X., Xiao, L., & Shi, J. (2021). Uncertainty Modeling for Multi center Autism Spectrum Disorder Classification Using Takagi-Sugeno-Kang Fuzzy Systems. *IEEE Transactions on Cognitive and Developmental Systems*.

Huynh-Thu, Q., & Ghanbari, M. (2008). Scope of validity of PSNR in image/video quality assessment. In *Electronics Letters* (Vol. 44, pp. 800-801): Institution of Engineering and Technology.

Jia, D., Zheng, G., Qu, B., & Khan, M. K. (2011). A hybrid particle swarm optimization algorithm for high-dimensional problems. *Computers & Industrial Engineering, 61*, 1117-1122.

Kapur, J. N., Sahoo, P. K., Wong, A. K. J. C. v., graphics,, & processing, i. (1985). A new method for gray-level picture thresholding using the entropy of the histogram. *29*, 273-285.

Karpagam, M., Geetha, K., & Rajan, C. (2020). A modified shuffled frog leaping algorithm for scientific workflow scheduling using clustering techniques. *Soft Computing, 24*, 637-646.

Kennedy, J., & Eberhart, R. (1995). Particle swarm optimization. In *Proceedings of ICNN'95 - International Conference on Neural Networks* (Vol. 4, pp. 1942-1948 vol.1944).

Kordestani, H., Zhang, C., Masri, S. F., & Shadabfar, M. (2021). An empirical time‐domain trend line‐based bridge signal decomposing algorithm using Savitzky–Golay filter. *Structural Control and Health Monitoring, 28*, e2750.

Kotte, S., Pullakura, R. K., & Injeti, S. K. (2018). Optimal multilevel thresholding selection for brain MRI image segmentation based on adaptive wind driven optimization. *Measurement: Journal of the International Measurement Confederation, 130*, 340-361.

Lai, X., & Zhou, Y. (2020). Analysis of multiobjective evolutionary algorithms on the biobjective traveling salesman problem (1, 2). *Multimedia Tools and Applications, 79*, 30839-30860.

Li, S., Chen, H., Wang, M., Heidari, A. A., & Mirjalili, S. (2020). Slime mould algorithm: A new method for stochastic optimization. *Future Generation Computer Systems, 111*, 300-323.

Liang, D., Zhan, Z.-H., Zhang, Y., & Zhang, J. (2019). An efficient ant colony system approach for new energy vehicle dispatch problem. *IEEE Transactions on Intelligent Transportation Systems, 21*, 4784-4797.

Liang, J. J., Qin, A. K., Suganthan, P. N., & Baskar, S. (2006). Comprehensive learning particle swarm optimizer for global optimization of multimodal functions. *IEEE Transactions on Evolutionary Computation, 10*, 281-295.

Liang, X., Cai, Z., Wang, M., Zhao, X., Chen, H., & Li, C. (2020). Chaotic oppositional sine–cosine method for solving global optimization problems. *Engineering with Computers*, 10.1007/s00366-00020-01083-y.

Liu, L., Zhao, D., Yu, F., Heidari, A. A., Li, C., Ouyang, J., Chen, H., Mafarja, M., Turabieh, H., & Pan, J. (2021). Ant colony optimization with Cauchy and greedy Levy mutations for multilevel COVID 19 X-ray image segmentation. *Computers in Biology and Medicine, 136*, 104609.

Liu, X.-F., Zhan, Z.-H., & Zhang, J. (2021). Resource-Aware Distributed Differential Evolution for Training Expensive Neural-Network-Based Controller in Power Electronic Circuit. *Ieee Transactions on Neural Networks and Learning Systems*, DOI: 10.1109/TNNLS.2021.3075205.

Liu, Y., Chong, G., Heidari, A. A., Chen, H., Liang, G., Ye, X., Cai, Z., & Wang, M. (2020). Horizontal and vertical crossover of Harris hawk optimizer with Nelder-Mead simplex for parameter estimation of photovoltaic models. *Energy Conversion and Management, 223*, 113211.

Liu, Y., Heidari, A. A., Ye, X., Chi, C., Zhao, X., Ma, C., Turabieh, H., Chen, H., & Le, R. (2021). Evolutionary shuffled frog leaping with memory pool for parameter optimization. *Energy Reports, 7*, 584-606.

Mallipeddi, R., Suganthan, P. N., Pan, Q. K., & Tasgetiren, M. F. (2011). Differential evolution algorithm with ensemble of parameters and mutation strategies. *Applied Soft Computing, 11*, 1679-1696.

Manikandan, S., Ramar, K., Iruthayarajan, M. W., & Srinivasagan, K. G. J. M. (2014). Multilevel thresholding for segmentation of medical brain images using real coded genetic algorithm. *47*, 558-568.

Meng, A.-b., Chen, Y.-c., Yin, H., & Chen, S.-z. (2014). Crisscross optimization algorithm and its application. *Knowledge-Based Systems, 67*, 218-229.

Mirjalili, S., & Lewis, A. (2016). The Whale Optimization Algorithm. *Advances in Engineering Software,*

95, 51-67.
Mirjalili, S., Mirjalili, S. M., & Lewis, A. (2014). Grey wolf optimizer. *Advances in Engineering Software, 69*, 46-61.
Muzaffar M. Eusuff, K. E. L. (2003). Optimization of Water Distribution Network Design Using the Shuffled Frog Leaping Algorithm *Journal of Water Resources Planning and Management, 129*, 201.
N. H. Awad, M. Z. A., P. N. Suganthan, J. J. Liang and B. Y. Qu. (2016). Problem Definitions and Evaluation Criteria for the CEC 2017 Special Session and Competition on Single Objective Real-Parameter Numerical Optimization. In: Zhengzhou University, Nanyang Technological University.
Pare, S., Kumar, A., Bajaj, V., & Singh, G. K. (2016). A multilevel color image segmentation technique based on cuckoo search algorithm and energy curve. *Applied Soft Computing Journal, 47*, 76-102.
Pei, H., Yang, B., Liu, J., & Chang, K. (2020). Active Surveillance via Group Sparse Bayesian Learning. *IEEE Transactions on Pattern Analysis and Machine Intelligence*, DOI: 10.1109/TPAMI.2020.3023092.
Peng, H., Wang, J., Pérez-Jiménez, M. J., & Shi, P. (2013). A novel image thresholding method based on membrane computing and fuzzy entropy. *Journal of Intelligent and Fuzzy Systems, 24*, 229-237.
Qin, A. K., Huang, V. L., & Suganthan, P. N. (2009). Differential Evolution Algorithm With Strategy Adaptation for Global Numerical Optimization. *IEEE Transactions on Evolutionary Computation, 13*, 398-417.
Qin, J., Wang, C., & Qin, G. (2019). A Multilevel Image Thresholding Method Based on Subspace Elimination Optimization. *Mathematical Problems in Engineering, 2019*.
Qiu, S., Hao, Z., Wang, Z., Liu, L., Liu, J., Zhao, H., & Fortino, G. (2021). Sensor Combination Selection Strategy for Kayak Cycle Phase Segmentation Based on Body Sensor Networks. *Ieee Internet of Things Journal*, https://doi.org/10.1109/JIOT.2021.3102856.
Qiu, S., Zhao, H., Jiang, N., Wu, D., Song, G., Zhao, H., & Wang, Z. (2021). Sensor network oriented human motion capture via wearable intelligent system. *International Journal of Intelligent Systems*, https://doi.org/10.1002/int.22689.
Saber, A., Sakr, M., Abo-Seida, O. M., Keshk, A., & Chen, H. (2021). A Novel Deep-Learning Model for Automatic Detection and Classification of Breast Cancer Using the Transfer-Learning Technique. *IEEE Access, 9*, 71194-71209.
Sheng, H., Wang, S., Zhang, Y., Yu, D., Cheng, X., Lyu, W., & Xiong, Z. (2020). Near-online tracking with co-occurrence constraints in blockchain-based edge computing. *IEEE Internet of Things Journal, 8*, 2193-2207.
Socha, K., & Dorigo, M. (2008). Ant colony optimization for continuous domains. *European Journal of Operational Research, 185*, 1155-1173.
Storn, R., & Price, K. (1997). Differential Evolution – A Simple and Efficient Heuristic for global Optimization over Continuous Spaces. *Journal of Global Optimization, 11*, 341-359.
Storn, R., & Price, K. J. J. o. G. O. (1997). Differential Evolution – A Simple and Efficient Heuristic for global Optimization over Continuous Spaces. *11*, 341-359.
Tang, K., Xiao, X., Wu, J., Yang, J., & Luo, L. (2017). An improved multilevel thresholding approach based modified bacterial foraging optimization. *Applied Intelligence, 46*, 214-226.
Tang, K., Yuan, X., Sun, T., Yang, J., & Gao, S. (2011). An improved scheme for minimum cross entropy threshold selection based on genetic algorithm. *Knowledge-Based Systems, 24*, 1131-1138.
Tsai, C. Y., Liu, T. Y., & Chen, W. C. (2012). A novel histogram-based multi-threshold searching algorithm for multilevel colour thresholding. *International Journal of Advanced Robotic Systems, 9*.
Tu, J., Chen, H., Wang, M., & Gandomi, A. H. (2021). The Colony Predation Algorithm. *Journal of Bionic Engineering, 18*, 674-710.
Tu, J., Lin, A., Chen, H., Li, Y., & Li, C. (2019). Predict the entrepreneurial intention of fresh graduate students based on an adaptive support vector machine framework. *Mathematical Problems in Engineering, 2019*, 1-16.
W, D., JJ, X., YJ, S., & HM, Z. (2020). An Effective Improved Co-evolution Ant Colony Optimization Algorithm with Multi-Strategies and Its Application. *International Journal of Bio-Inspired Computation*, 16(13): 158–170.
Wang, M., & Chen, H. (2020). Chaotic multi-swarm whale optimizer boosted support vector machine for medical diagnosis. *Applied Soft Computing, 88*, 105946.
Wang, M., Zhang, Q., Chen, H., Heidari, A. A., Mafarja, M., & Turabieh, H. (2021). Evaluation of constraint in photovoltaic cells using ensemble multi-strategy shuffled frog leading algorithms. *Energy*

Conversion and Management, 244, 114484.
Wang, Y., Zhang, G., & Zhang, X. (2019). Multilevel Image Thresholding Using Tsallis Entropy and Cooperative Pigeon-inspired Optimization Bionic Algorithm. *Journal of Bionic Engineering, 16*, 954-964.
Wolpert, D. H., & Macready, W. G. (1997). No free lunch theorems for optimization. *IEEE Trans on Evolutionary Computation, 1*, 67-82.
Wu, Z., Li, C., Cao, J., & Ge, Y. (2020). On Scalability of Association-rule-based recommendation: A unified distributed-computing framework. *ACM Transactions on the Web (TWEB), 14*, 1-21.
Wu, Z., Li, G., Shen, S., Cui, Z., Lian, X., & Xu, G. (2021). Constructing dummy query sequences to protect location privacy and query privacy in location-based services. *World Wide Web, 24*, 25-49.
Wu, Z., Li, R., Xie, J., Zhou, Z., Guo, J., & Xu, X. (2020). A user sensitive subject protection approach for book search service. *Journal of the Association for Information Science and Technology, 71*, 183-195.
Wu, Z., Shen, S., Lian, X., Su, X., & Chen, E. (2020). A dummy-based user privacy protection approach for text information retrieval. *Knowledge-Based Systems, 195*, 105679.
Wu, Z., Shen, S., Zhou, H., Li, H., Lu, C., & Zou, D. (2021). An effective approach for the protection of user commodity viewing privacy in e-commerce website. *Knowledge-Based Systems, 220*, 106952.
Wu, Z., Wang, R., Li, Q., Lian, X., & Xu, G. (2020). A location privacy-preserving system based on query range cover-up for location-based services. *IEEE Transactions on Vehicular Technology, 69*.
Xu, Y., Chen, H., Luo, J., Zhang, Q., Jiao, S., & Zhang, X. (2019). Enhanced Moth-flame optimizer with mutation strategy for global optimization. *Information Sciences, 492*, 181-203.
Xue, X., Chen, Z., Wang, S., Feng, Z., Duan, Y., & Zhou, Z. (2020). Value Entropy: A Systematic Evaluation Model of Service Ecosystem Evolution. *Ieee Transactions on Services Computing*, DOI: 10.1109/TSC.2020.3016660.
Yang, X.-S. (2010). A New Metaheuristic Bat-Inspired Algorithm. In J. R. González, D. A. Pelta, C. Cruz, G. Terrazas & N. Krasnogor (Eds.), *Nature Inspired Cooperative Strategies for Optimization (NICSO 2010)* (pp. 65-74). Berlin, Heidelberg: Springer Berlin Heidelberg.
Yang, Y., Chen, H., Heidari, A. A., & Gandomi, A. H. (2021). Hunger games search: Visions, conception, implementation, deep analysis, perspectives, and towards performance shifts. *Expert Systems with Applications, 177*, 114864.
Yang, Z., Li, K., Guo, Y., Ma, H., & Zheng, M. (2018). Compact real-valued teaching-learning based optimization with the applications to neural network training. *Knowledge-Based Systems, 159*, 51-62.
Yang, Z., & Wu, A. (2019). A non-revisiting quantum-behaved particle swarm optimization based multilevel thresholding for image segmentation. *Neural Computing and Applications*.
Yin, F., Xue, X., Zhang, C., Zhang, K., Han, J., Liu, B., Wang, J., & Yao, J. (2021). Multifidelity genetic transfer: an efficient framework for production optimization. *SPE J*, 1-22.
Yin, P. Y. (2007). Multilevel minimum cross entropy threshold selection based on particle swarm optimization. *Applied Mathematics and Computation, 184*, 503-513.
Ying, C., Ying, C., & Ban, C. (2018). A performance optimization strategy based on degree of parallelism and allocation fitness. *EURASIP Journal on Wireless Communications and Networking, 2018*, 1-8.
Yu, C., Chen, M., Cheng, K., Zhao, X., Ma, C., Kuang, F., & Chen, H. (2021). SGOA: annealing-behaved grasshopper optimizer for global tasks. *Engineering with Computers*, 10.1007/s00366-00020-01234-00361.
Zeng, G.-Q., Xie, X.-Q., Chen, M.-R., & Weng, J. (2019). Adaptive population extremal optimization-based PID neural network for multivariable nonlinear control systems. *Swarm and Evolutionary Computation, 44*, 320-334.
Zenggang, X., Zhiwen, T., Xiaowen, C., Xue-min, Z., Kaibin, Z., & Conghuan, Y. (2019). Research on Image Retrieval Algorithm Based on Combination of Color and Shape Features. *Journal of Signal Processing Systems*, 1-8.
Zhang, H., Cai, Z., Ye, X., Wang, M., Kuang, F., Chen, H., Li, C., & Li, Y. (2020). A multi-strategy enhanced salp swarm algorithm for global optimization. *Engineering with Computers*, 1-27.
Zhang, L., Zhang, L., Mou, X., & Zhang, D. (2011). FSIM: A Feature Similarity Index for Image Quality Assessment. *IEEE Transactions on Image Processing, 20*, 2378-2386.
Zhang, L., Zou, Y., Wang, W., Jin, Z., Su, Y., & Chen, H. (2021). Resource Allocation and Trust Computing for Blockchain-Enabled Edge Computing System. *Computers & Security*, 102249

Zhang, X., Du, K.-J., Zhan, Z.-H., Kwong, S., Gu, T.-L., & Zhang, J. (2019). Cooperative coevolutionary bare-bones particle swarm optimization with function independent decomposition for large-scale supply chain network design with uncertainties. *Ieee Transactions on Cybernetics, 50*, 4454-4468.

Zhang, X., Fan, M., Wang, D., Zhou, P., & Tao, D. (2021). Top-<italic>k</italic> Feature Selection Framework Using Robust 0–1 Integer Programming. *Ieee Transactions on Neural Networks and Learning Systems, 32*, 3005-3019.

Zhang, X., Jiang, R., Wang, T., & Wang, J. (2021). Recursive Neural Network for Video Deblurring. *Ieee Transactions on Circuits and Systems for Video Technology, 31*, 3025-3036.

Zhang, X., Wang, D., Zhou, Z., & Ma, Y. (2019). Robust low-rank tensor recovery with rectification and alignment. *IEEE Transactions on Pattern Analysis and Machine Intelligence, 43*, 238-255.

Zhang, X., Wang, J., Wang, T., Jiang, R., Xu, J., & Zhao, L. (2021). Robust feature learning for adversarial defense via hierarchical feature alignment. *Information Sciences, 560*, 256-270.

Zhang, X., Wang, T., Wang, J., Tang, G., & Zhao, L. (2020). Pyramid channel-based feature attention network for image dehazing. *Computer Vision and Image Understanding, 197*, 103003.

Zhang, Y., Liu, R., Wang, X., Chen, H., & Li, C. (2020). Boosted binary Harris hawks optimizer and feature selection. *Engineering with Computers*, 1-30.

Zhao, D., Liu, L., Yu, F., Heidari, A. A., & Chen, H. J. E. S. w. A. (2020). Ant colony optimization with horizontal and vertical crossover search: Fundamental visions for multi-threshold image segmentation. *http://aliasgharheidari.com*, 114122.

Zhao, D., Liu, L., Yu, F., Heidari, A. A., Wang, M., Liang, G., Muhammad, K., & Chen, H. (2021). Chaotic random spare ant colony optimization for multi-threshold image segmentation of 2D Kapur entropy. *Knowledge-Based Systems, 216*, 106510.

Zhao, D., Liu, L., Yu, F., Heidari, A. A., Wang, M., Oliva, D., Muhammad, K., & Chen, H. (2021). Ant colony optimization with horizontal and vertical crossover search: Fundamental visions for multi-threshold image segmentation. *Expert Systems with Applications, 167*, 114122.

Zhao, H., Liu, H., Xu, J., Deng, W. J. I. T. o. i., & measurement. (2019). Performance prediction using high-order differential mathematical morphology gradient spectrum entropy and extreme learning machine. *IEEE Transactions on Instrumentation & Measurement*, https://doi.org/10.1109/TIM.2019.2948414.

Zhao, X., Li, D., Yang, B., Chen, H., Yang, X., Yu, C., & Liu, S. (2015). A two-stage feature selection method with its application. *Computers & Electrical Engineering, 47*, 114-125.

Zhao, X., Zhang, X., Cai, Z., Tian, X., Wang, X., Huang, Y., Chen, H., & Hu, L. (2019). Chaos enhanced grey wolf optimization wrapped ELM for diagnosis of paraquat-poisoned patients. *Computational biology and chemistry, 78*, 481-490.

Zhou, W., Bovik, A. C., Sheikh, H. R., & Simoncelli, E. P. (2004). Image quality assessment: from error visibility to structural similarity. *IEEE Transactions on Image Processing, 13*, 600-612.

Zhou, W., Lv, Y., Lei, J., & Yu, L. (2021). Global and Local-Contrast Guides Content-Aware Fusion for RGB-D Saliency Prediction. *IEEE Transactions on Systems, Man, and Cybernetics: Systems, 51*, 3641-3649.

Zhou, Y., Yang, X., Ling, Y., & Zhang, J. (2018). Meta-heuristic moth swarm algorithm for multilevel thresholding image segmentation. *Multimedia Tools and Applications, 77*, 23699-23727.